JOURNAL OF GEOPHYSICAL RESEARCH, VOL. 103, NO. A8, PAGES 17,391–17,410, AUGUST 1, 1998

Relationship of topside ionospheric ion outflows to auroral forms and precipitation, plasma waves, and convection observed by Polar

M. Hirahara,[1,2,3,4] J. L. Horwitz,[1] T. E. Moore,[2,5] G. A. Germany,[1] J. F. Spann,[2] W. K. Peterson,[6] E. G. Shelley,[6] M. O. Chandler,[2] B. L. Giles,[2] P. D. Craven,[2] C. J. Pollock,[7] D. A. Gurnett,[8] J. S. Pickett,[8] A. M. Persoon,[8] J. D. Scudder,[8] N. C. Maynard,[9] F. S. Mozer,[10] M. J. Brittnacher,[11] and T. Nagai[12]

Abstract. The POLAR satellite often observes upflowing ionospheric ions (UFIs) in and near the auroral oval on southern perigee (~5000 km altitude) passes. We present the UFI features observed by the thermal ion dynamics experiment (TIDE) and the toroidal imaging mass angle spectrograph (TIMAS) in the dusk-dawn sector under two different geomagnetic activity conditions in order to elicit their relationships with auroral forms, wave emissions, and convection pattern from additional POLAR instruments. During the active interval, the ultraviolet imager (UVI) observed a bright discrete aurora on the duskside after the substorm onset and then observed a small isolated aurora form and diffuse auroras on the dawnside during the recovery phase. The UFIs showed clear conic distributions when the plasma wave instrument (PWI) detected strong broadband wave emissions below ~10 kHz, while no significant auroral activities were observed by UVI. At higher latitudes, the low-energy UFI conics gradually changed to the polar wind component with decreasing intensity of the broadband emissions. V-shaped auroral kilometric radiation (AKR) signatures observed above ~200 kHz by PWI coincided with the region where the discrete aurora and the UFI beams were detected. The latitude of these features was lower than that of the UFI conics. During the observations of the UFI beams and conics, the lower-frequency fluctuations observed by the electric field instrument were also enhanced, and the convection directions exhibited large fluctuations. It is evident that large electrostatic potential drops produced the precipitating electrons and discrete auroras, the UFI beams, and the AKR, which is also supported by the energetic plasma data from HYDRA. Since the intense broadband emissions were also observed with the UFIs, the ionospheric ions could be energized transversely before or during the parallel acceleration due to the potential drops.

1. Introduction

Over the past 2 decades, a number of observational surveys have demonstrated that the ionosphere is a significant plasma source for the Earth's magnetosphere [e.g., *Ghielmetti et al.*, 1979; *Johnson*, 1979; *Balsiger et al.*, 1980; *Horwitz*, 1982; *Shelley et al.*, 1982; *Waite et al.*, 1985; *Moore et al.*, 1985; *Chappell et al.*, 1987; *Pollock et al.*, 1990]. The acceleration processes injecting ionospheric ions into the magnetosphere include auroral parallel electrostatic potential drops, wave-particle interactions, and ambipolar electric fields [e.g., *Hultqvist et al.*, 1988; *Chang et al.*, 1986; *André et al.*, 1990;

[1]Center of Space Plasma, Aeronomy, and Astrophysics Research, University of Alabama in Huntsville.

[2]Space Sciences Laboratory, NASA Marshall Space Flight Center, Huntsville, Alabama.

[3]Department of Earth and Planetary Physics, Faculty of Science, University of Tokyo, Hongo, Bunkyo-ku, Tokyo, Japan.

[4]Now at Department of Physics, College of Science, Rikkyo University, Nishi-Ikebukuro, Toshima-ku, Tokyo, Japan.

Paper number 97JA02668.
0148-0227/98/97JA-02668$09.00

[5]Now at Interplanetary Physics Branch, NASA Goddard Space Flight Center, Greenbelt, Maryland.

[6]Lockheed Martin Space Physics Laboratory, Palo Alto, California.

[7]Instrumentation and Space Research Division, Southwest Research Institute, San Antonio, Texas.

[8]Department of Physics and Astronomy, University of Iowa, Iowa City.

[9]Mission Research Corporation, Nashua, New Hampshire.

[10]Space Sciences Laboratory, University of California, Berkeley.

[11]Geophysics Program, University of Washington, Seattle.

[12]Planetary and Earth Sciences, Tokyo Institute of Technology, Ookayama, Meguro-ku, Tokyo, Japan.

Crew et al., 1990; *Hultqvist*, 1996; *Banks and Holzer*, 1968; *Nagai et al.*, 1984; *Lockwood et al.*, 1985; *Chandler et al.*, 1991; *Abe et al.*, 1993a, b]. These processes lead to escaping ion flows observed by polar-orbiting satellites and sounding rockets which may be classified as field-aligned upward flowing ion (UFI) beams, transversely accelerated ions (TAIs) and/or UFI conics, and the polar wind.

It has been demonstrated that the ejected flux of the outflowing ionospheric ions energized by the auroral processes increases during active periods [e.g., *Yau et al.*, 1984, 1985; *Kondo et al.*, 1990]. Corresponding enhancements of ionospheric ion content have been found in the magnetotail, and the clear correlations of the heavy ion flux and density with the geomagnetic activity have been revealed by many works [e.g., *Peterson et al.*, 1981; *Sharp et al.*, 1981, 1982; *Young et al.*, 1982; *Lennartsson et al.*, 1985].

Polar-orbiting satellite data have also revealed detailed characteristics and processes, forming discrete electron precipitation accelerated by parallel electrostatic potential drops [e.g., *Frank and Ackerson*, 1971; *Bosqued et al.*, 1986]. The ionospheric ions are evidently accelerated upward in the field-aligned direction by the same potential drops [e.g., *Collin et al.*, 1981; *Reiff et al.*, 1988; *Lundin and Hultqvist*, 1989; *Lu et al.*, 1992].

The process(es) generating the TAIs and the UFI conics have also been investigated intensively from both theoretical and observational perspectives. Simultaneous observations of UFIs or TAIs and enhanced low-frequency plasma waves, suggesting a relationship, were reported by a number of authors [e.g., *Kintner and Gorney*, 1984; *Moore et al.*, 1986; *Kintner et al.*, 1989; *André et al.*, 1987, 1988; *Peterson et al.*, 1988; *Chen et al.*, 1990; *Erlandson et al.*, 1994; *Norqvist et al.*, 1996; *Kintner et al.*, 1996]. *Liu et al.* [1994a] proposed that field-aligned currents are associated with low-energy conics, but not with low-energy beams. Also, *Liu et al.* [1994b] showed a correlation of UFI signatures with convection reversals on the basis of the DE 1 observations on the nightside and suggested that the convection reversal itself could provide a free energy source for the perpendicular heating of the UFI conics. *Moore et al.* [1996] recently presented sounding rocket observations of low-energy ions and electric fields to examine the perpendicular energization of O^+ in an auroral arc. These studies have indicated that the perpendicular energization of the ionospheric ions is associated with the wave activity, field-aligned currents, and plasma convection features. The fine-scale correlations of the UFI conics with some of the features described above were examined in some of the previous works. However, more comprehensive results are needed to examine general relationships of the conics to the auroral environment.

It is important to also investigate the relationships of UFIs to characteristics of nearby auroral forms. The global features of auroral forms, such as brightness, type (diffuse or discrete), and spatial distribution, vary drastically according to geomagnetic activity level [e.g., *Akasoku*, 1963, 1964; *Craven and Frank*, 1985, 1987; *Elphinstone and Hearn*, 1992, 1993, and references therein]. Recently, *Elphinstone et al.* [1995a] and *Henderson et al.* [1996] investigated the detailed global auroral features on the basis of Viking image data. From the viewpoint of the global supply processes of the ionospheric ions from the auroral and polar regions into the magnetosphere, the relationships of the UFI conics and beams, and the polar wind, to the auroral forms and the associated parallel electrostatic potential drop should be examined further using comprehensive spacecraft observations.

On the basis of measurements of energetic and thermal plasma, auroral images, and wave emissions, *Horwitz et al.* [1992] showed the comprehensive observations made by DE 1 to discuss the outflowing O^+ components in the polar cap magnetosphere. *Yamamoto et al.* [1993] studied auroral images, plasma features, and electric and magnetic field data observed by Akebono in the nightside auroral region during active times. They demonstrated that the conic signatures were located in higher latitudes than the bright emissions from the discrete auroras. In their results, the inverted-V electrons carrying the majority of the upward field-aligned currents were coincident with the discrete auroras and the convection reversal, and the UFI beams were often observed with the inverted-V electrons. These charged particles were concluded to have been accelerated by the parallel potential drops above and below the satellite, while neither high- nor low-frequency wave activity was evident. In the Akebono results, the convection reversal is colocated with the bright auroral forms associated with the inverted V structures of electrons and ions.

Recently, detailed examinations of auroral structures for the late stages of substorms were shown by *Elphinstone et al.* [1995b, c]. The ion energy spectra and the auroral images indicated that some signatures of the UFI conics at the poleward edge of the auroral oval existed together with the most poleward discrete aurora arc in the nightside sector of 2100-0300 MLT. They also concluded that the inverted-V events occurred in the main UV oval at lower latitudes than the discrete aurora. The convection reversal observed on the dawnside did not coincide with the discrete auroras, which differs from the premidnight observations reported by *Yamamoto et al.* [1993]. The image data used in these studies were useful for examining the global distributions of aurora. However, further investigations are needed to establish more definite relations between UFIs and auroral features which drastically vary in space and time.

Moreover, it is well known that the high-frequency electromagnetic plasma wave emissions are related to discrete electron precipitation events and auroral arcs. *Benson and Calvert* [1979] and *Green et al.* [1979] reported the correlation of auroral kilometric radiation (AKR) with the inverted-V electrons, rather than with plasma sheet electrons. The relation between the AKR and the highly structured precipitating electrons accelerated by parallel electrostatic potential drop was also confirmed on the basis of the ISIS 1 and Viking data in greater detail [*Benson et al.*, 1980; *Ungstrup et al.*, 1990]. *Menietti et al.* [1993] presented fine structure relationships seen in the AKR and plasma observations with DE 1 data. *Huff et al.* [1988], on the other hand, studied the correlation of the AKR signatures with auroral formation and demonstrated a strong correlation between the location of the AKR source regions and the regions of bright auroral optical emissions.

Although each of these studies is important to discuss the

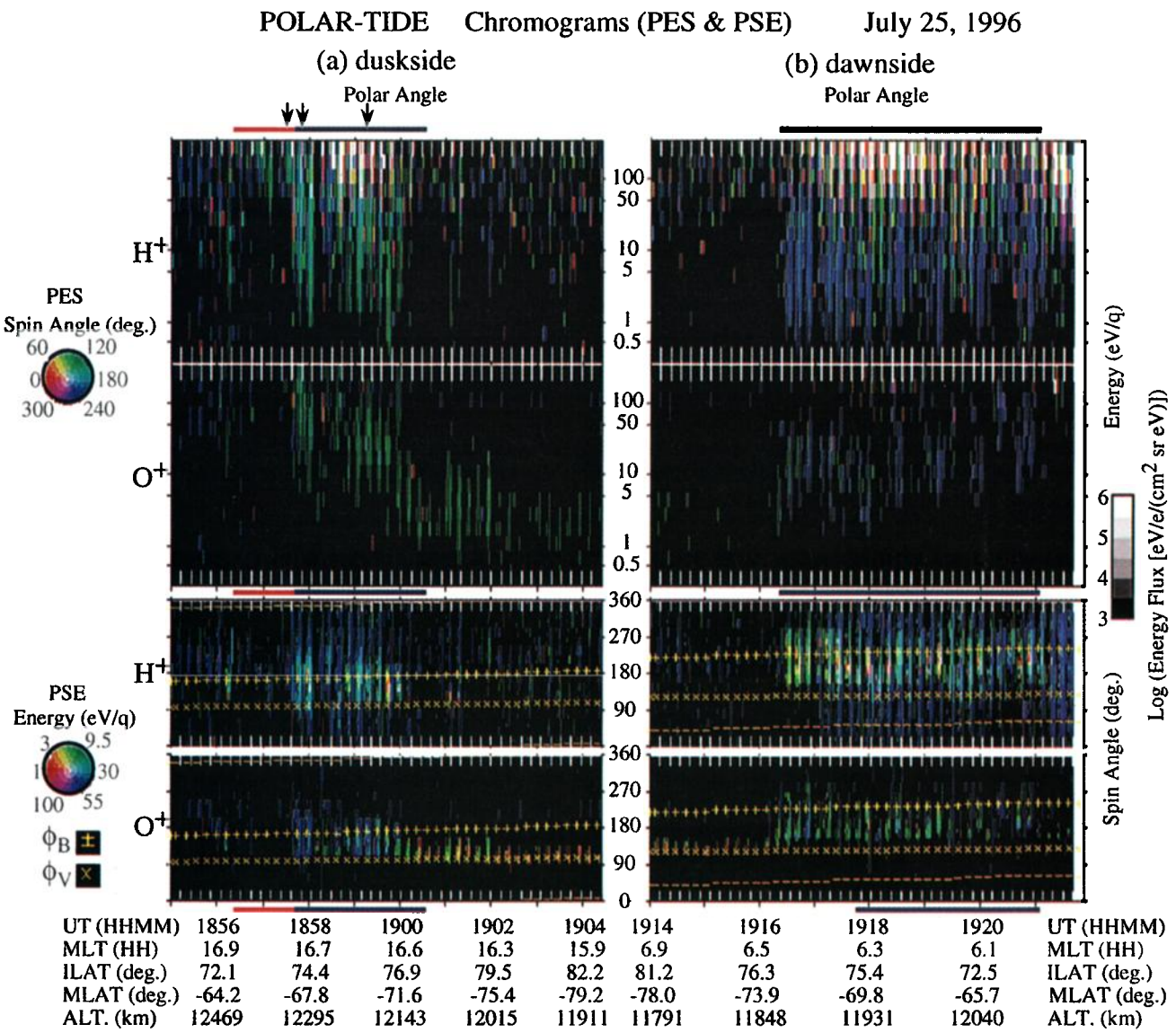

Plate 1. Chromograms for low-energy H^+ and O^+ ions observed by TIDE on the (a) duskside and (b) dawnside southern perigee pass on July 25, 1996: PES chromograms showing energy-time (*E-t*) spectrograms consisting of energy-polar angle bins and PSE chromograms showing variations of the angular distributions. The scales of the ion energy and flux are logarithmic. See the text about the chromogram format. At the bottom of the chromograms, universal time (UT, in hours and minutes), magnetic local time (MLT, in hours), invariant latitude (ILAT, in degrees), magnetic latitude (MLAT, in degrees), and geocentric altitude (ALT., in kilometers) of POLAR are shown. The red and blue underlines near the abscissas indicate the intervals of the UFI beam (red) and conic (blue) signatures. The velocity distributions during the intervals indicated by downward arrows at the top are shown in Plates 2 and 5.

ionospheric supply process(es) which might be related to the other phenomena, there have been few studies comprehensively reporting the relation of the low-energy upflowing ions (UFIs) with both auroral and plasma wave emissions on the basis of the simultaneous observations by instruments with high sensitivity and time/spatial resolution. In particular, there have been few plasma instruments capable of measuring thermal and suprathermal ions with high time resolution and fully three-dimensional angular coverage. The recently launched POLAR mission achieves high-quality ion measurements with newly developed technique for the study of upgoing ionospheric ions. POLAR also produces images of auroral emissions with high-time resolution and high-performance filters in ultraviolet, visible, and X ray wavelengths. This paper is devoted to the examination of the UFI signatures and their relationships to fine-scale auroral features, wave emissions, and convection patterns on the basis of observations by the POLAR satellite.

2. Instrumentation and Data Display

In this paper, we will present comprehensive plasma, field, and auroral imaging observations during two intervals obtained by several instruments on the POLAR satellite within

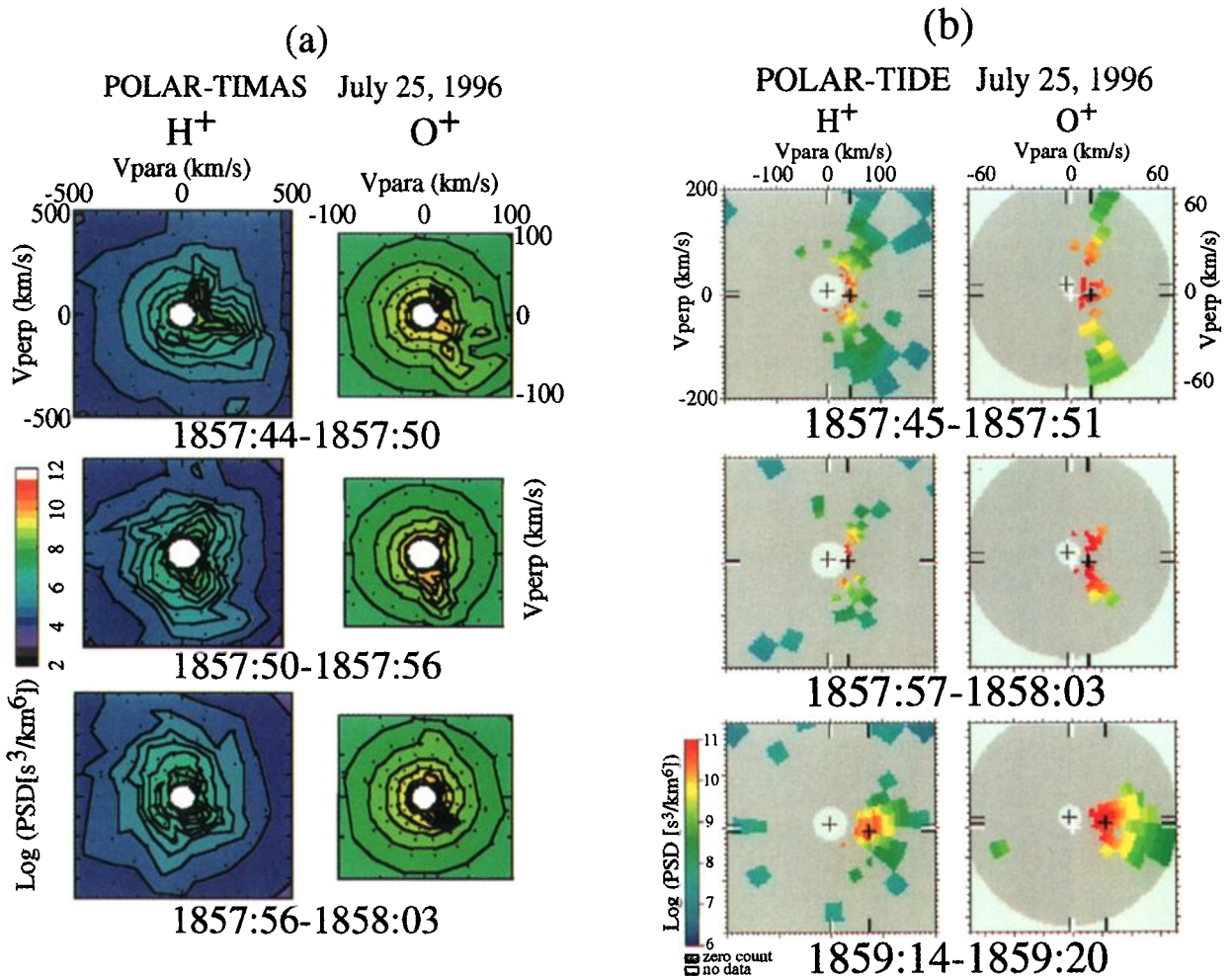

Plate 2. Velocity distribution functions of the low-energy H^+ and O^+ conics and beams observed by TIDE and TIMAS on the duskside. The plane of the two-dimensional cuts of the distributions contains the magnetic field.

the southern hemisphere near the perigee (~5000 km). The focus is on low-energy ions measured by the Thermal Ion Dynamics Experiment (TIDE [*Moore et al.*, 1995]) which has seven identical sensors, each of which consists of two segments: an energy analyzer using an electrostatic mirror and a retarding potential analyzer, and a mass spectrometer employing a time-of-flight technique. By the combination of the wide polar angle (157.5°) covered by the seven channels and the satellite spin angle divided into 32 sectors, the instrument measures fully three-dimensional velocity distributions of major ion species (H^+, He^{2+}, He^+, O^+, and some molecular ions) in the magnetosphere with good angular resolution (11.25°×22.5°). The energy range for this study is 0.1-300 eV, which is divided into 16 steps on a logarithmic scale, although the full energy coverage is 0.1-450 eV/q. The time resolution is 6 s, which is the spin period.

We present the TIDE data here through several versions of a new data display format, "chromograms." The horizontal axis of each chromogram is observation time (UT; universal time in hours and minutes). The "PES" (polar angle in abscissa, energy in ordinate, spin angle in color code) chromogram, as seen at the top of Plate 1, shows the polar angle and energy distributions of the ion flux in the horizontal and the vertical axes, respectively, in each bin separated by white tick marks. The flux range is from 10^3 to 10^6 eV/(s sr cm^2 eV), as indicated by a vertical brightness bar on the right hand of the chromograms. The spin angle information is color coded, as shown by a color wheel on the left hand of the PES chromograms.

The "PSE" (polar angle in abscissa, spin angle in ordinate, energy in color code) chromogram shows the time variation of the polar and spin angles, expressing energy and ion flux with a color code on the left hand and a brightness level on the right hand, respectively. It should be noted that lower-energy (0.1-3 eV/q) and higher-energy (30-300 eV/q) ions are depicted with red and blue, respectively. Yellow plus and minus symbols in each bin show the magnetically parallel and antiparallel directions, respectively, and cross symbols indicate the direction of the satellite ram motion.

Typical UFI conics would show relatively wide spreads in the energy and angular axes in PES chromograms and large circular distributions with a hole at the center around yellow plus marks in PSE chromograms, and UFI beams should be seen as thin and short stripes in a narrow energy range in the PES chromograms and as small closed dots at yellow plus marks in the PSE chromograms. Low-energy

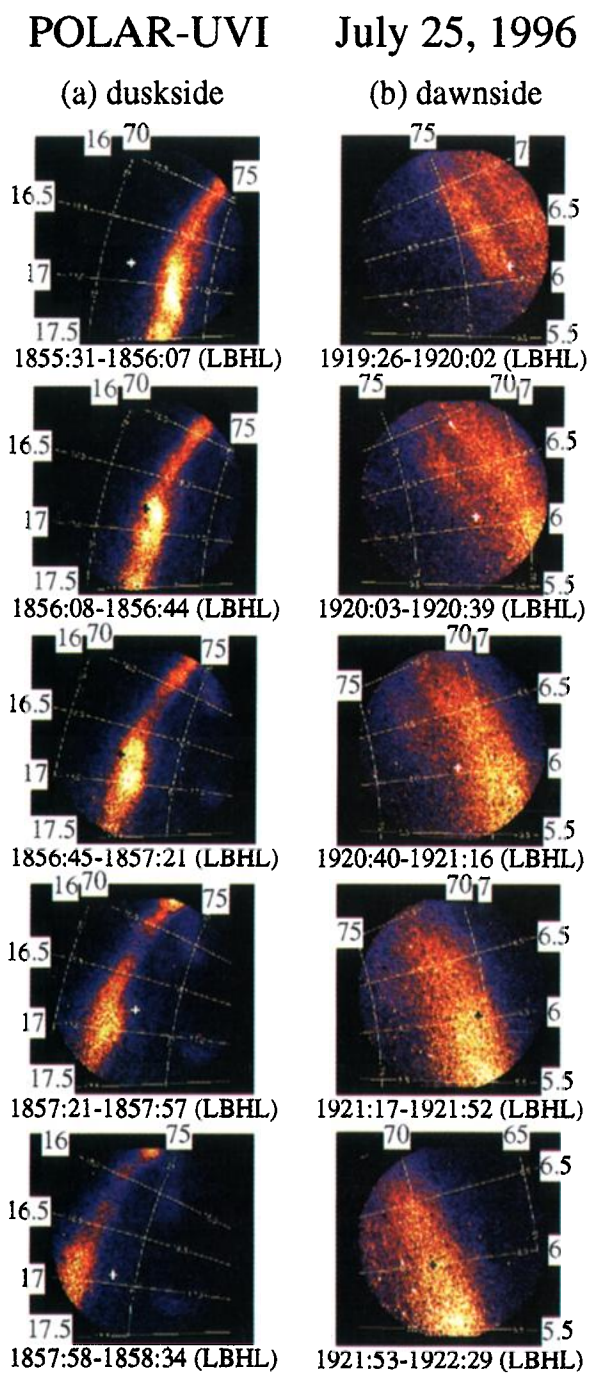

Plate 3. Five successive auroral images observed on the (a) duskside and (b) dawnside by UVI on July 25, 1996. The exposure time and the type of filter used then are given below each image. The values of MLT and MLAT are also shown near the rim of each image. A cross mark in each of images indicates the footpoint of satellite at the start time of exposure.

polar wind component would be measured near the satellite ram direction (yellow cross marks) due to the fast satellite speed near the perigee and should be plotted with red (low energy) in the PSE chromograms.

In the case of Plate 1a, the upward direction along the magnetic field changed roughly from 150° to 200° of the spin angle, as seen in the PSE chromogram at the bottom. A color variation from blue to red indicates that the energy of the upgoing low-energy ionospheric ions changed from ~50 to ~3 eV/q, corresponding to a change from conics to polar wind. The precipitating energetic ions with isotropic pitch angle distributions are shown with gray or white in the PES chromograms.

It is also important to compare the thermal ion data from TIDE with higher-energy ion composition measurement by the Toroidal Imaging Mass Angle Spectrograph (TIMAS [*Shelley et al.*, 1995]). For the TIMAS data used in this paper, the energy range of the fully three-dimensional energy spectra of H^+ and O^+ are 15 eV/q to 22 keV/q divided into 28 logarithmically spaced steps separated into two interleaving groups of 14 steps, although the full energy coverage is 15 eV/q to 33 keV/q. The two groups are sampled on successive spins. The intrinsic angular resolution is 11.25°×11.25°. The limited telemetry band width requires onboard processing into data products that are averaged over different regions of the mass-energy-angle space covered by the instrument. Data from the medium resolution distribution with 6 s, 14 energy steps, and 22×22 degree resolution are presented here. The high-energy ion and electron data are provided from the HYDRA experiment [*Scudder et al.*, 1995]. The energy range of the ion and electron data shown here is ~20 eV/q to ~20 keV/q. TIMAS and HYDRA cover full pitch angle ranges by the wide field of views and the spin motion as well as TIDE. We present velocity distribution contour plots from TIMAS in addition to the omnidirectional E-t spectrograms from TIMAS and HYDRA.

The UltraViolet Imager (UVI [*Torr et al.*, 1995]) consists of five filters including a solar spectral filter, three mirrors, and a CCD system. UVI can detect auroral emissions of the wavelength from 130 to 170 nm with four wavelength ranges. The time resolution is 37 s, and the field of view and the angular resolution are a circular 8° and 0.03°, respectively. From the low-altitude pass near perigee, UVI provides images with spatial resolution sufficient to investigate fine auroral structures, although the area sampled in each image is somewhat restricted. The global coverage and spatial resolution are approximately 980×963 km^2 and 4.9×4.3 km^2, respectively, at the altitude of 1 R_E.

The wave activities associated with some auroral phenomena seen in the TIDE and UVI data were obtained by the Plasma Wave Investigation (PWI [*Gurnett et al.*, 1995]). We study the spectra observed by the sweep frequency receiver (SFR) and the multichannel analyzer (MCA), which are connected to a short (14 m), two-sphere electric antenna (E_z) aligned along the spacecraft spin axis and a magnetic loop antenna with its axis oriented in the spacecraft spin plane. The frequency ranges of SFR are divided to five bands: 0.026-0.2, 0.2-1.6, 1.7-12.6, 13-100, 100-808 kHz. The time resolutions of SFR is 32 s/spectra in the logarithmic mode. The frequency range and resolution of MCA are 5.6 Hz to 311 kHz and 20 channels on a logarithmic scale, respectively, for electric field measurements, and the time resolution is 1.3 s/spectra. The frequency range of the MCA data presented in this paper is 5.6 - 100 kHz.

The data from the Electric Field Instrument (EFI [*Harvey et al.*, 1995]) on POLAR is useful for examining the plasma convection pattern and low-frequency fluctuations in

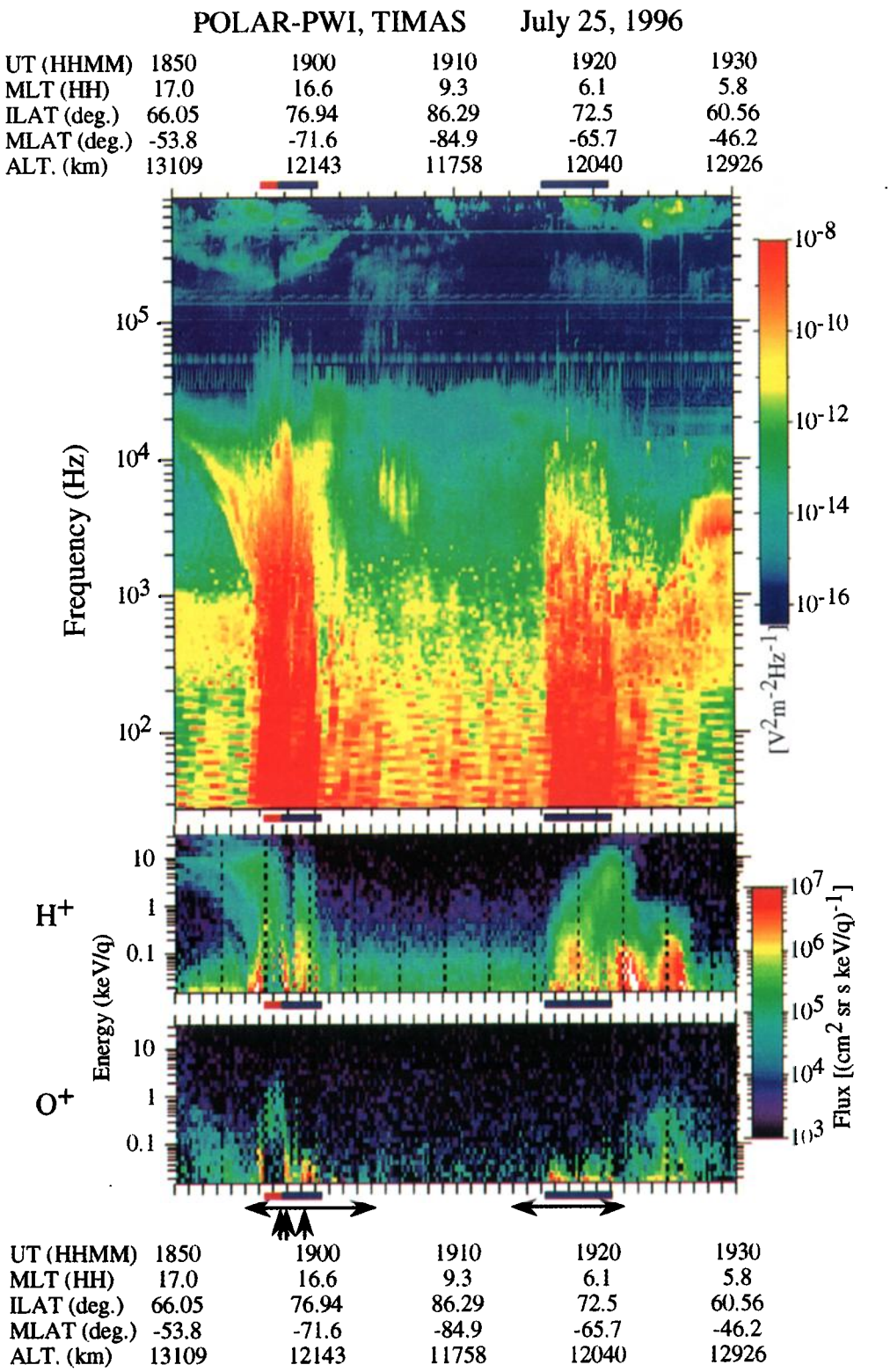

Plate 4. Simultaneous observations by PWI (top panel) and TIMAS (bottom two panels: H^+ and O^+) on July 25, 1996. The PWI panel shows a frequency-time (*f-t*) spectrogram of the electric field component observed by PWI-SFR. The ordinate shows the wave frequency (hertz) on logarithmic scale. The TIMAS data are energy-time (*E-t*) spectrograms. The ordinates are ion energies (keV/*q*) on logarithmic scale. The intensity of the wave emissions and the fluxes of ions are expressed in logarithmic scales, as shown in the color codes on the right hand of the spectrograms. The red and blue underlines near the abscissas are correspondent to the underlines in Plate 1, indicating the UFI beams (red) and conics (blue). The intervals indicated by two horizontal lines with arrows at the bottom are the same with those of the TIDE chromograms in Plate 1. The velocity distributions during the intervals indicated by upward arrows are shown in Plates 2 and 5. The orbital information is also displayed similarly to that of Plate 1.

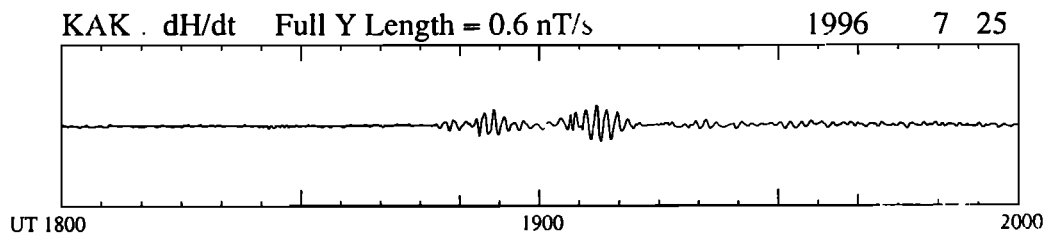

Figure 1. Pi 2 pulsation data during 1800-2000 UT around the POLAR observations on July 25, 1996, obtained in Japanese ground magnetometer station, Kakioka (KAK). The first onset signature is seen at 1847 UT, followed by second enhancement of the pulsation around 1907 UT when POLAR was in the high-latitude polar cap. During the POLAR crossing in the dawnside auroral oval, some small-amplitude pulsations were observed.

the electric field. We present the dc component and high-time resolution data of electric fields measured by a short (14 m) and two long (100 and 130 m) sphere anntenas. We also consider the features of the low-frequency electric field fluctuations observed by EFI.

The Pi 2 pulsation data from a ground magnetometer in the Kakioka station are shown to indicate ongoing geomagnetic activity. The key parameter data measured by the Magnetic Field Instrument (MFI [*Lepping et al.*, 1995]) and the Solar Wind Experiment (SWE [*Ogilvie et al.*, 1995]) on the Wind satellite are briefly described to indicate the IMF conditions before and during the POLAR observations presented here.

3. Observations

3.1. July 25, 1996, 1850-1930 UT: A Geomagnetically Active Interval

The POLAR data on July 25, 1996, provide us with a unique opportunity to investigate the detailed features of the upflowing ionospheric ions and their relationship with the auroral activities, wave emissions, and convection observed in and near the duskside and the dawnside auroral oval near the perigee in the southern hemisphere during a geomagnetically active interval. The IMF B_z component was negative (~ -4 nT), and the solar wind speed was approximately 385 km/s until $\sim$1830 UT, according to the Wind observations upstream of $\sim$187 R_E from the Earth. Although the geomagnetic condition does not seem active (Kp=2_+ during 1800-2100 UT), the Kakioka ground geomagnetic station located at the postmidnight sector (MLT=0300-0500) observed clear Pi 2 pulsations enhanced because of two successive substorm onsets during the POLAR observations, as plotted in Figure 1. Injections of high-energy ($\sim$1 MeV) electrons were also seen in the geosynchronous satellite (GMS 4) data, although the enhancement of the flux was only by a factor of 2.

Plate 1 shows two sets of PES (top two panels) and PSE (bottom two panels) chromograms of the H^+ and O^+ ions observed by TIDE on the (Plate 1a) duskside and (Plate 1b) dawnside. POLAR moved from the duskside at 1600-1700 MLT to the dawnside at 0600-0700 MLT in the southern polar region. In the duskside auroral oval during 1855:50-1900:30 UT, TIDE observed intense UFI beam and conic signatures in H^+ and O^+, as shown by the red (beam) and blue (conics) horizontal lines near the abscissas (also see spectrograms and velocity distribution plots of higher-energy ions by TIMAS in Plates 4 and 5 to identify the UFI beam). It is obvious that the flux of the H^+ conics was larger than that of O^+, while the O^+ peak energy was slightly higher than that of H^+. Around 1900 UT, the O^+ energy gradually decreased from several tens of eV to several eV with increasing latitude. During the conics, TIDE observed the low-energy ($>\sim$50 eV/q) tail of the velocity distributions of the energetic magnetospheric protons, which was rather isotropic, as seen in the H^+ chromogram. This is a useful feature in the TIDE chromograms for roughly identifying the auroral oval location. The high-energy UFI beams of H^+ and O^+ ions were also observed by TIMAS before the duskside conic features, which are presented in more detail later to examine the relationships with the auroral forms and high-frequency plasma wave activity.

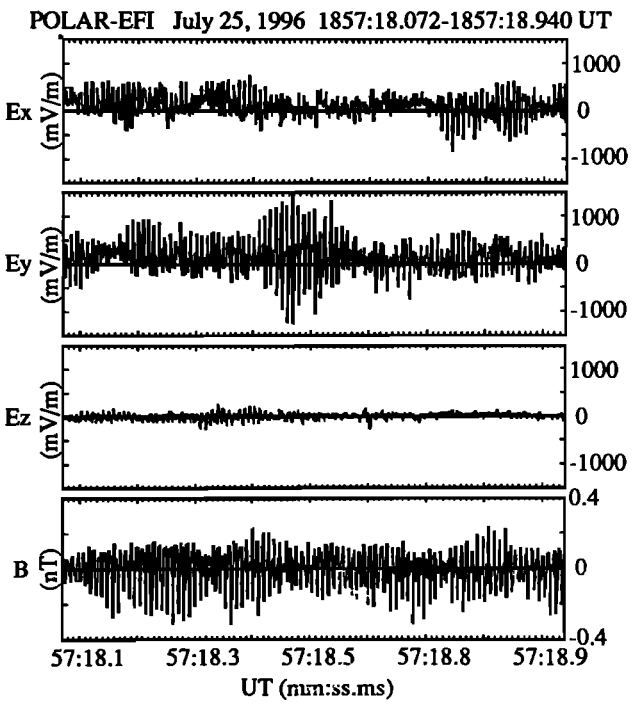

Figure 2. Examples of the electric and magnetic field data observed near the center of the inverted-V event and the discrete aurora. Top three panels show the E_x and E_y components perpendicular to the magnetic field and the E_z component parallel to the magnetic field measured by the dipole anntenas. The magnetic field component observed by the search coil magnetometer also shown at the bottom.

The variations of the angular distributions of the upgoing ionospheric ions (conics and polar wind) are depicted in the PSE-type chromograms. The chromograms show some ring-like features with a hole at the center, which are signatures of conics, particularly near 1857:50 UT on the duskside. While the intense ion fluxes of the H^+ and O^+ conics were observed around the upward direction parallel to the local magnetic field before ~1900 UT, the polar wind component after ~1902 UT was measured nearly in the ram direction. In the PES chromograms on the duskside, the typical energies of O^+ varied from ~50 eV in the conic features during 1857:30-1859:30 UT to a few eV in the polar wind component as rammed by the satellite motion after ~1902 UT. The energy of the O^+ component observed by TIDE is consistent with the satellite-ram energy for O^+, for the satellite speed of approximately 7 km/s near perigee. The energy and angular characteristics of the low-energy upflowing ionospheric ions gradually changed from the conic distribution at lower latitudes to the thermal upwelling ion component rammed by the satellite motion in the polar cap (~1902-1916 UT). The polar wind consisted mainly of O^+ ions, although H^+ outflow might exist at energies lower than those whose sampling was allowed by satellite potential of a few volts.

Plate 2 shows the velocity distributions of the H^+ and O^+ conics and beams observed by TIMAS (Plate 2a) and TIDE (Plate 2b) on the duskside. In both types of plots, the right hand directions of the horizontal axes are the upward directions along the local magnetic field lines. During three successive intervals of the TIMAS observations, the H^+ and O^+ conics had conical angles of ~30°-50°, which are consistent with the TIDE results during the same period. On the other hand, a third example of TIDE measurement in Plate 2 suggests that there was a small electrostatic potential drop at 1859:14-1859:20 UT during the observations of the higher-latitude conics, indicating that the low-energy UFI beam could be a consequence of the parallel acceleration. Similar features showing alternating UFI conics and beams were often seen in the TIDE data. Most of them were instantaneously detected and embedded especially during the observation periods of the conics.

Next, we present the spatial distribution of auroral forms observed by UVI with high spatial and time resolutions in order to consider the relationship with the upflowing ion signatures (conics and beams). A bright auroral form can be seen at ~73°-75° in the UVI data during the duskside observation, as shown in Plate 3a. The brightness of the duskside auroral form seems to gradually decrease according to the decrease of the amplitude of the Pi 2 pulsations after 1855 UT and/or the elapse time after the first onset at ~1842 UT. It also seems that the discrete aurora was located at slightly lower latitudes than the region with the UFI conics during

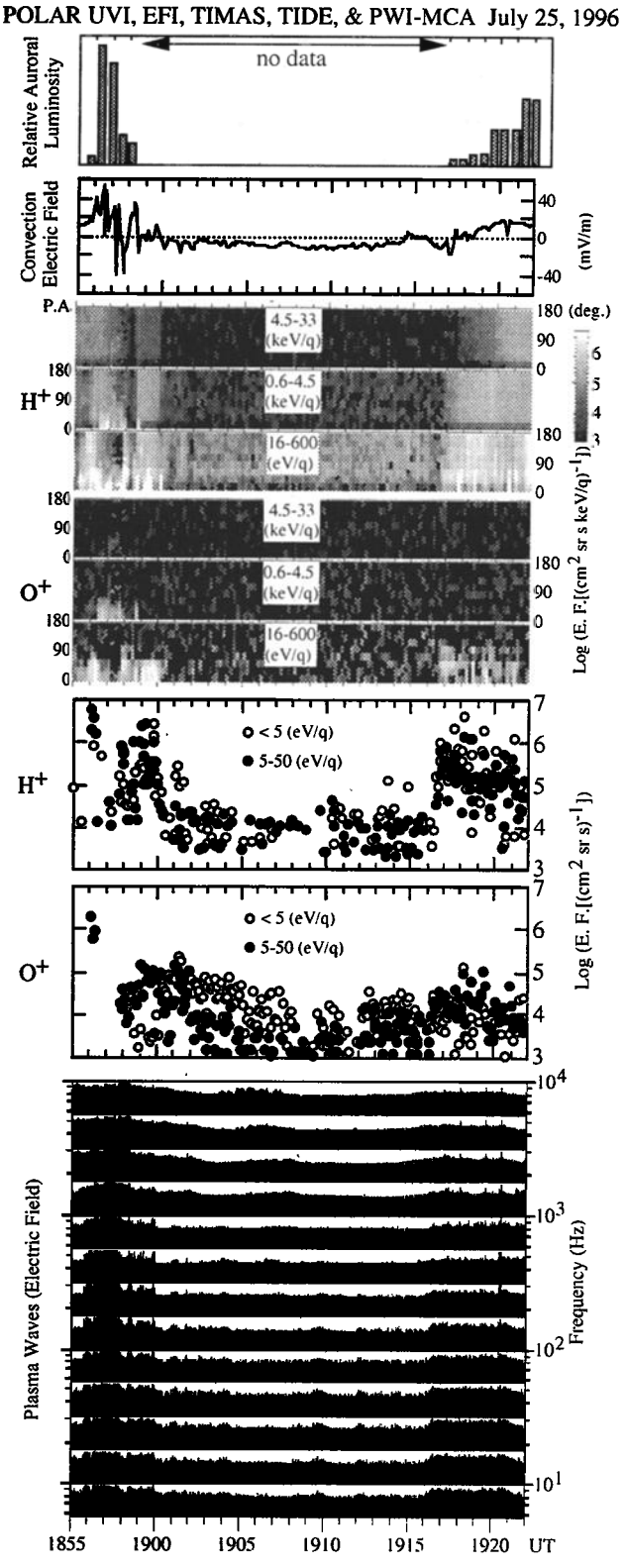

Figure 3. POLAR data for the July 25 event. From the top, relative auroral luminosity at satellite footpoint on a linear scale, dc electric field spin-plane component along the satellite velocity vector, pitch angle-time (α-t) spectrograms of H^+ and O^+ sorted into three energy ranges (4.5-33 keV/q, 0.6-4.5 keV/q, and 16-600 eV/q from the top in each subset), energy fluxes of H^+ and O^+ integrated over the upward direction (open circles for ions of <5 eV/q, closed for 5-50 eV/q), and electric field components of plasma waves. The positive and negative values (millivolts per meter) in the dc electric fields roughly correspond the sunward and antisunward convection directions. The ordinate of six α-t spectrograms is the pitch angle (0°-180°), and the energy fluxes are depicted by brightness shown in a right hand vertical bar.

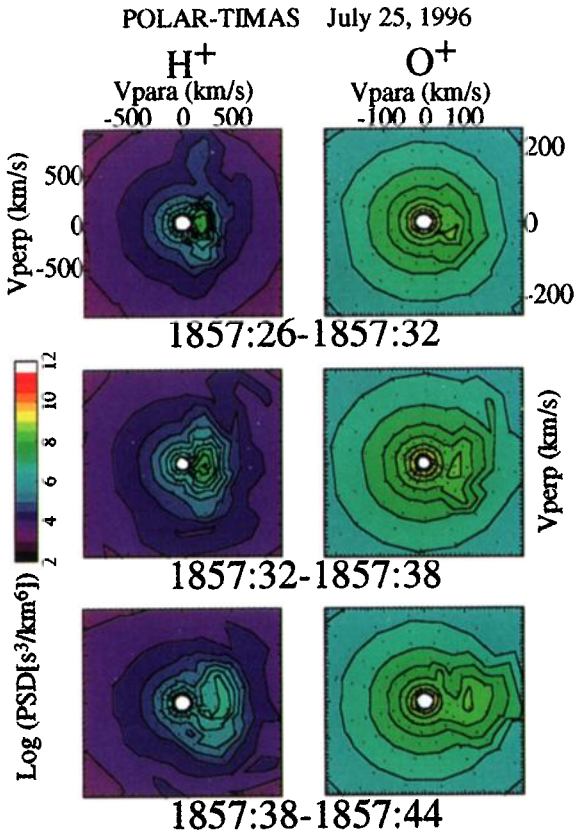

Plate 5. Velocity distribution functions of the H^+ and O^+ beams observed by TIMAS, similar to Plate 2a, but for the UFI beams during the inverted-V signature.

1857:40-1859:30 UT. Neither other discrete nor diffuse auroras were evidently observed at latitudes higher than 68°, although auroral forms might be present at lower latitudes. It is possible that the main auroral oval composed of the diffuse auroras extended at ~10° lower latitude than the active auroral form (for example, see auroral images during the substorms shown by *Yamamoto et al.* [1993] and *Elphinstone et al.* [1995b]).

From the top panel of Plate 4, a frequency-time (*f-t*) spectrogram of the electric field component observed by PWI-SFR and energy-time (*E-t*) spectrograms of H^+ and O^+ observed by TIMAS are shown. The *f-t* and *E-t* spectrograms indicate electric field power spectral densities and energy fluxes of H^+ and O^+, respectively. Blue horizontal lines near the abscissas indicate the conic observation intervals, and two thin lines with arrows at the bottom show the interval of the TIDE chromograms in Plate 1. Red lines indicate the interval during which the high-energy beam-like UFIs were observed by TIDE and TIMAS. The UFI conics during 1857:40-1859:30 UT discussed in Plates 1 and 2 were associated with the enhanced auroral hiss emissions and broadband electrostatic emissions observed by PWI in and near the auroral oval, as indicated by the blue lines, while the lower-energy polar wind component existed in the polar cap with no significant wave activities after 1900 UT. The energy variation of the conics showed a correlation with the lower-frequency (<~10 kHz) wave emissions. The strong correlation between the UFI beams and conics and the occurrence of low-frequency auroral hiss emissions and broadband electrostatic emissions suggests that the ionospheric ions could be energized by interactions of ions with, for instance, ion cyclotron and lower hybrid waves, as proposed theoretically and observationally by many authors [e.g., *Crew et al.*, 1990; *André et al.*, 1990; *Norqvist et al.*, 1996, references therein].

On the other hand, the broadband emissions were also intense for a few minutes before 1858 UT, and the EFI data also show that the most intense electric field fluctuations were located at lower latitudes than the conics. Figure 2 shows an example of the lower-frequency electric and magnetic fields observed by EFI and the search coil magnetometer during the UFI beam event. It should be noted that the amplitudes of the electric field components perpendicular to the magnetic field were quite large (~200-1500 mV/m) at the frequency of ~100 Hz. The magnetic field components were relatively small (~0.1-0.3 nT) in the amplitudes, suggesting that these waves were mainly electrostatic, as discussed by *Temerin et al.* [1996]. The ionospheric ions could be significantly energized in the perpendicular direction by these large amplitude waves also in the parallel potential drop as well as in the regions where the clear conics were observed. It is plausible that the ionospheric ions were further accelerated by the parallel electrostatic potential drop, after or during the perpendicular heating caused by the wave-particle interactions in the topside ionosphere.

In the bottom two panels of Plate 4, the energetic ion composition data from TIMAS show the ion (H^+ and O^+) "inverted-V" signatures with "hole" structures around 1857 UT, as indicated by the red lines. The peak energies of the H^+ and O^+ were comparable at several hundreds of eV/*q*, and the UFI beams coexisted with higher-energy diffuse H^+ signatures. It should be noted that the high-energy UFI beam region in the range ILAT=72°-74° is nearly coincident with the bright auroral region.

Plate 5 shows the distribution functions of the high-energy UFI beams observed by TIMAS for three successive measurements of the 6-s snapshots. The peaks of the UFI beams are obviously seen in the field-aligned direction at the velocity ranges of ~200-450 km/s and ~70-120 km/s for the H^+ and O^+ ions, respectively. Just after these UFI beams were detected, TIDE and TIMAS began to detect the UFI conics, as shown in Plates 1 and 2.

In the vicinity of the duskside auroral oval, the AKR signature was observed at the high-frequency ranges at >200 kHz, as shown at the top portion of Plate 4. The *f-t* spectrogram also shows the double AKR emissions which were separate at the higher- (>~500 kHz) and lower- (<~400 kHz) frequency ranges. These features are also confirmed in the magnetic field component data from the magnetic loop antenna (the data are not shown here). The AKR emission at the lower-frequency range showed a clear V-shaped signature, which implies that the satellite crossed or encountered the source field line at ~1857 UT, as discussed by *Gurnett* [1991]. The center of the V-shaped AKR emission was located at slightly lower latitudes than the conics in Plate 2, and existed in the region where the high-energy UFI beams and the discrete auroral forms were observed by TIMAS and UVI, respectively.

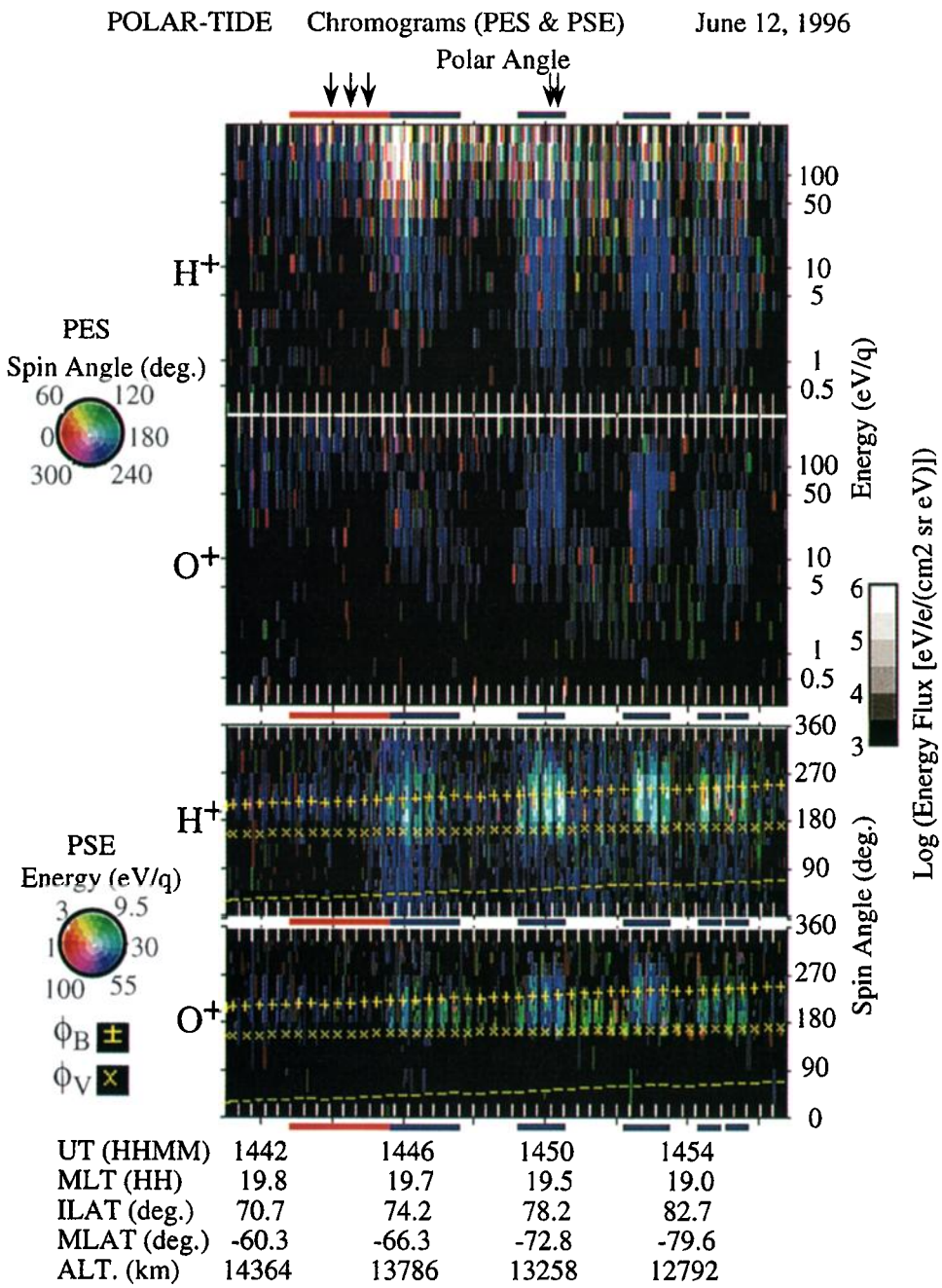

Plate 6. TIDE chromograms for H^+ and O^+ on the duskside on June 12, 1996, similar to Plate 1. The red and blue underlines indicate the UFI beams (red) and conics (blue). The velocity distributions during the intervals indicated by downward arrows at the top are shown in Plates 7 and 9.

The above results from the plasma, image, and wave instruments indicate that the bright discrete aurora was produced by inverted-V electrons accelerated by the parallel electrostatic potential drop at lower latitudes than the UFI conic signatures. When $\mathbf{E}_{\parallel}$ existed not only above but also below the satellite altitude, the conics energized by the plasma waves at the ionospheric altitudes may have been accelerated further to higher energy ranges. It is realistic to expect that the ionospheric ion components were finally accelerated upward to the peak energy of several keV by the full parallel electrostatic potential drop associated with the auroral structure.

Figure 3 shows the correlations among the auroral luminosity, electric field spin-plane component along the satellite velocity vector, upgoing ion fluxes, and wave emissions (the global convection pattern will be discussed in detail after we present the dawnside observations). A drop of the low-energy H^+ and O^+ fluxes integrated over <5 and 5-50 eV/q is seen during ~1856:30-1858 UT. A similar feature can be found in the pitch angle-time (α-t) spectrograms of H^+ and O^+ of 16-600 eV/q. These features are due to the large parallel acceleration of the upgoing ions by an electrostatic potential drop below the satellite. During this period, high-energy ions (beams, also see Plate 5) were observed in the upward direc-

tion, as seen in the α-t spectrograms for 0.6-4.5 keV/q O^+, and the intense auroral emission was also recorded, as plotted in the top panel of Figure 3. Before and after this period, the low-energy (< 50 eV/q) ion fluxes were enhanced, which are consistent with the features in the α-t spectrograms of the lowest-energy range. The flux enhancements of the high- and low-energy upgoing ions had a good correlation with the broadband wave emissions mainly of < 1 kHz frequencies in the bottom panel. Although the H^+ flux was generally larger than that for O^+, only the O^+ component of <5 eV/q had significant fluxes for about five minutes after 1902 UT because the satellite ram motion was effective to detect the heavy ions of the polar wind component. It is reasonable that the O^+ component had no correlation with the wave emissions. Three α-t spectrograms of H^+ indicate that the energetic magnetospheric proton component had isotropic distributions.

The conics were clearly observed during the interval of 1916:30-1921:30 UT in the dawnside region on the same POLAR pass, as presented in Plate 1b. As is evident in the O^+ component in the PES and PSE chromograms, the upgoing ionospheric ion angular and energy features varied from signatures of the polar wind to conics. These latitudinal variations were similar to those on the duskside. Compared with the duskside conics, the dawnside conics were more widely distributed in latitude (ILAT~77.5°-70°), and the ion fluxes and energies were lower. The low-energy tail of the magnetospheric proton precipitation was seen at the higher-energy range than the conics, also similar to the duskside case. This component can be confirmed in the H^+ E-t spectrogram of TIMAS data in Plate 4. Unfortunately, the TIDE operation mode changed to a safe mode at ILAT~70°, prohibiting indications of outflowing ion signatures which might have existed at lower latitudes.

The auroral activities on the dawnside had wide spatial distributions, as seen in the UVI images of Plate 3b, and the auroral forms were mainly observed at lower latitudes than 70° at 0600 MLT. The emissions of the main auroral oval around MLAT~67° were relatively steady, while the isolated aurora at MLAT~69°-70° rapidly became faint and finally vanished before POLAR crossed the region. Because the dawnside observations were made mainly during the recovery phase after two onset signatures, it is reasonable to consider that the higher-latitude auroral emissions gradually decreased during the activity. The higher-latitude aurora seems small and transient in the POLAR image data. A similar type of double auroral oval was reported by *Elphinstone et al.* [1995b, c]. We consider that the main auroral oval was formed not by discrete arcs but by a diffuse type of aurora because no drastic fluctuations in the electric field data were seen corresponding to the lower-latitude auroral activity.

Although the emissions of the dawnside plasma waves and the discrete auroras were somewhat weaker than those on the duskside, the spatial distribution of the auroral hiss emission and broadband electrostatic emission was wider and corresponded well to the conic signatures, as seen in Plate 4. The PWI data show that the broadband wave activity decreased before ~1922 UT at ILAT~70°. The low-frequency electric field data from EFI also indicate no significant fluctuations after ~1921 UT. It therefore is logical to consider that neither significant perpendicular heating nor parallel acceleration of the ionospheric ions occurred at lower latitudes than ILAT~70° in the main auroral oval. Although TIMAS observed the enhanced H^+ and O^+ fluxes at the low-energy range around 1922-1923 and 1925-1926 UT of ILAT<70°, as seen in the E-t spectrograms of Plate 4, we believe that these were diffuse ion components at lower latitudes in the plasma sheet.

The AKR signature observed on the dawnside was different from that on the duskside. In particular, the maximum intensity of the dawnside AKR appears to be stronger than that on the duskside, as seen in the PWI plot of Plate 4. The magnetic field component measured by the loop antenna is consistent with these characteristics. The center of the AKR on the dawnside was located noticeably equatorward of the region where the clear conics and the intense broadband wave emissions were observed, and the characteristic frequency was >400 kHz. As contrasted with the correlations in the duskside observations, the dawnside dominant AKR emission at lower latitudes was isolated from significant features found in the plasma, aurora, and electric field measurements. On the other hand, a small AKR signature during 1918-1920 UT would be related to the isolated aurora because the AKR emission was observed simultaneously when the footpoint of the satellite was inside the isolated aurora, as seen in Plates 3 and 4.

The top panel of Figure 3 shows that the intense emissions from the diffuse auroras on the dawnside were observed mainly at low latitudes after 1921 UT, while the conic signatures and flux enhancements had a good correlation with the broadband electrostatic emissions of <1 kHz at higher latitudes during 1916:30-1921:30 UT. No ion beam nor conic signatures were found in the high-energy range (>0.6 keV/q) on the dawnside.

The second panel of Figure 3 shows the dc electric field spin-plane component along the satellite velocity vector for estimating the convection pattern features. The positive and negative values are consistent with sunward and antisunward convection for this dusk-dawn orbit. The convection was almost antisunward in the polar cap from ~1900 to ~1917 UT, although there was a small excursion in the sunward direction during ~1914-1916 UT. The steady sunward convection seen at lower latitudes on both duskside and dawnside is consistent with the typical pattern during southward IMF, as reported by *Heppner and Maynard* [1987]. During the periods of the steady sunward convection, energetic magnetospheric protons with isotropic distributions were observed, as seen in the α-t spectrograms. In the bright discrete aurora and the UFI beam environment on the duskside during ~1856-1858 UT, the dc electric field component was drastically enhanced and variable, ranging between 40 and −40 mV/m. Following this highly structured variation, a shorter-term positive enhancement was also seen during 1858-1859 UT. The high-energy UFI beams were associated with the first larger variation, and the UFI conics were mainly observed during and after the second enhancement of the electric field. It is likely that the dominant convection flow reversal on the duskside occurred in the large parallel potential drop producing the auroral emissions and the UFI beams. On the other hand, although the dawnside region also displayed a convection re-

versal region near 1918 UT, no enhancements in the electric field component could be measured. This is consistent with the fact that the dawnside auroral oval near ~67° consisted primarily of diffuse auroras without discrete forms produced by a large electrostatic potential drop. Also, in the dawnside region, the conics were observed in the vicinity of the convection reversal during 1916-1921 UT.

3.2. June 12, 1996, 1420-1515 UT: A Geomagnetically Quiet Interval

POLAR observed multiple conic signatures during a geomagnetically quiet period on the southern duskside perigee pass on June 12, 1996, at 1420-1515 UT. The IMF was northward during this interval, with approximately IMF (B_x, B_y, B_z)=(0, −2, +2) nT when we take the Wind-Earth time lag before the POLAR observations into account, according to the MFI and SWE data. No large geomagnetic disturbances were seen in the frequency range of the Pi 2 pulsations observed by the Kakioka ground magnetometer during the interval of 1400-1600 UT at the midnight meridian. The *Kp* index ranged from 1_+ to 1_- during the 1200-1800 UT interval.

When POLAR crossed the auroral zone from lower latitudes to higher latitudes at MLT~2000-1830 and entered the polar cap, TIDE observed upflowing H^+ and O^+ conic signatures at ~1446, ~1450, ~1453, and ~1455 UT, as shown in the PES and PSE chromograms of Plate 6. It should be noted that the conics measured after ~1452 UT were located at higher latitudes than ~80°. The energies of the conics ranged from 1 eV to almost 1 keV, and the characteristic energy of the O^+ was uniformly higher than that of H^+, while the flux for O^+ was lower than that for H^+, as for the event of July 25. During the first interval of the conics observation approximately at 1446 UT, we can also see the significant flux of the diffuse components mainly consisting of H^+ at an energy range higher than ~50 eV. The magnetospheric energetic protons precipitated in the vicinity of the region, similar to the previous event. In this event, the conics coexisting with the energetic diffuse protons had a fainter flux than the conics observed at latitudes higher than 77°. This aspect will be discussed later from a viewpoint of the wave activity seen in the PWI and EFI data.

Two consecutive examples of the velocity distribution functions of the low-energy H^+ and O^+ conics and beams observed by TIDE are presented in Plate 7. The conic angle of the first H^+ example was in the range 30°-40°, slightly smaller than for the cases on July 25, which presumably means that the dominant heating perpendicular to the magnetic field occurred at lower altitudes. Also, the conic angle of O^+ was larger than that of H^+. The second example shows the low-energy beam-like UFIs observed in the next sample (6 s). The parallel bulk velocities of the UFI beams increased in both ion species, which was probably due to a small parallel potential drop, if the ΔE was approximately the same for both H^+ and O^+. TIDE frequently observes similar alternating occurrences of the conics and the beams at low-energy ranges in such perigee passes.

Plate 8 shows the time spectra of PWI, TIMAS, and HYDRA from the top. The data format used in each panel is similar to that of Plate 4. Blue and red horizontal lines, and a thin line with arrows near the abscissas indicate the repetitive conic observations, the high-energy beams, and the interval of the TIDE chromograms in Plate 6, respectively. In general, we observe correlations of the blue lines with other important auroral environment features, such as the broadband waves in the PWI data, the low-energy ion populations observed in the TIMAS and HYDRA data, and the discrete electron precipitation events in the HYDRA data.

At the top of Plate 8, the PWI data show two types of wave activity: V-shaped bands of AKR emission at high frequencies (>200 kHz) and auroral hiss emissions and broadband electrostatic bursts at frequencies below 20 kHz. The interval 1446-1448 UT seems to have slightly less intense broadband waves than the intervals for the other conics observed at higher latitudes, particularly at the frequency range above ~100 Hz. This could be associated with the observation that the conic flux at ~1447 UT was weaker than those of the higher-latitude conics. The EFI data also suggest that the amplitudes of the low-frequency electric field fluctuations were smaller during the first conic signatures than during the later cases, which is consistent with the higher-frequency PWI results.

The high-energy UFI beams were clearly observed by TIMAS just before the diffuse magnetospheric proton precipitation observed by TIDE at ~1446 UT. During the interval of the UFI beams, HYDRA observed a clear electron inverted-V event, which corresponds to the interval of the red lines in Plate 8. Although the peak energies of the UFI beams were higher than the instrumental limit of TIDE, the TIMAS data indicate that the peak energies were nearly the same for both ion species. Plate 9 shows three examples of the distribution functions of the high-energy UFI beams observed by TIMAS. During the UFI beams and the inverted-V electron structure, the parallel bulk velocity of the field-aligned ion beams increased and then decreased, as seen in Plate 9.

The AKR signature was observed only on the duskside, while the broadband emissions were seen in both duskside and dawnside auroral regions, as presented in the PWI plot. The dawnside auroral emissions detected by UVI were much fainter than the multiple auroral forms on the duskside and seems to be a latitudinally broad diffuse auroral form, like the lower-latitude auroral form in the dawnside case on July 25. Below, we discuss some possible relationships of the auroral activity with the inverted-V electrons and the AKR emissions. During this interval, unfortunately, the field of view of UVI missed the exact footpoint of POLAR that was located at latitudes similar to the field of view but at ~2000 MLT. Nevertheless, the UVI images are still useful for investigating the auroral environment in the vicinity of the UFI signatures. For studying the relationship of AKR intensity to auroral activity qualitatively, it is useful to infer the auroral luminosity near the footpoint from the UVI data through extrapolating the auroral alignment, because the AKR would propagate up and out from the vicinity of the auroral region [*Gurnett*, 1991]. The UVI auroral images presented in Plate 10 show at least two clear auroral forms in the UVI field of view, although the auroral luminosity was weak, which is consistent with the quiet geomagnetic condition. The auroras occurred intermittently and were restricted not only in the latitudinal but also the longitudinal directions, while they

were almost spatially stable. The multiple forms were located in different MLT regions. Equatorward of the auroras, faint diffuse auroral activity was observed.

Relating these measurements to the data from the plasma instruments, this region corresponds to intervals when significant fluxes of high-energy electrons and ions were observed by TIMAS and HYDRA, as shown in Plate 8. This indicates that the intense inverted-V electrons observed by HYDRA produced the discrete auroras observed partially at the nightside edge of the field of view by UVI. On the other hand, no significant auroral emissions would be observed in the poleward regions to be colocated with the intense UFI conic fluxes, although the field of view of UVI did not entirely cover the exact footpoint of the satellite and the very high-latitude region (ILAT>82°) where the highest-latitude conics were observed. In other words, no auroral features detectable by UVI could be seen in the polar cap, which is different from the plasma signatures.

In Plate 8, it should be noted that the lowest-frequency portion of the V-shaped AKR emission was located at slightly lower latitudes than the inverted-V electron event which should correspond to the discrete aurora (compare the red lines with the whole AKR signature). The ion signatures suggest that the parallel electrostatic potential drop was also present below the satellite altitude during the inverted-V electron events. Broadband wave emissions were also enhanced especially in the region poleward of the AKR center, which might imply that the ionospheric ions could have been heated perpendicularly below the potential drop. The AKR emission is more intense than that of the July 25 event. On the other hand, the geomagnetic activity was much lower in the present June 12 case than in the July 25 one. The auroral emission on the duskside was also weaker than for the bright discrete auroras seen on July 25.

Figure 4 shows the dc electric field spin-plane component along the satellite velocity vector, pitch angle distributions of energetic ions, thermal/suprathermal ion fluxes, and electric field components of plasma waves from the top. Similar to the July 25 event, a drop of low-energy (<50 eV/q) ion fluxes observed around ~1444 UT was due to the parallel acceleration, and the peak energies of the accelerated upgoing ion beams were beyond the upper energy limit of TIDE. At the same time, TIMAS observed the upgoing ions (beams, also see Plate 9) in the energy range of 0.6-4.5 keV/q, and then the flux enhancements due to the low-energy ion conics were repeatedly observed during 1445-1457 UT by TIDE. They are clearly seen also in the α-t spectrograms of the lowest energy range. These conic signatures were correlated well to the enhanced broadband wave emissions particularly of <1 kHz, as shown in the bottom panel. The H^+ flux of <50 eV/q was significantly larger than that for O^+, and the isotropic energetic protons were observed with the beam and conic signatures, which are similar to the features discussed in the July 25 event.

As seen in the dc electric field component in the top panel of Figure 4, local flow reversals or significant distortions of the convection pattern instantaneously occurred in the same regions where the conics were repetitively observed around 1446-1447 UT in the auroral oval, and at ~1450, ~1453, and 1454-1456 UT at higher latitudes. The detailed comparison

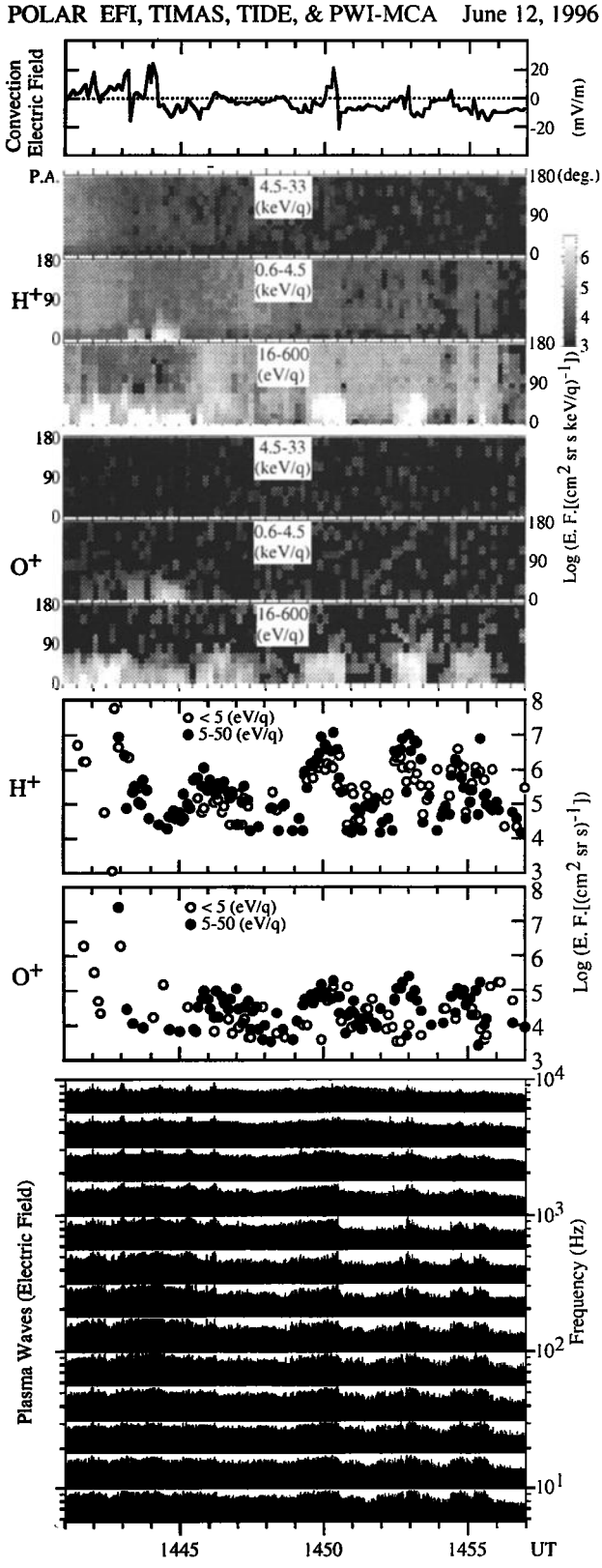

Figure 4. POLAR data for the June 12 event. Similar to Figure 3, but no auroral emission data.

suggests that magnetospheric electron precipitation events were observed along the negative gradients of the electric field. The enhancements of the low-frequency electric field fluctuations (not shown here) were also correlated with all of

the conic features and the strong broadband wave emissions measured by PWI. The structured electric field poleward of the main convection reversal at 1444 UT and the discrete plasma features might be associated with the auroras. On the other hand, the large enhancements of the dc electric field components were observed probably during the auroral oval crossing. It is likely that the enhanced electric fields were associated with the inverted-V electrons, and the ionospheric ions would be accelerated upward in the parallel direction equatorward from the conics.

4. Discussion

The distinct conic signatures were observed by TIDE and TIMAS in conjunction not only with the broadband wave emissions by PWI but also with the bursty electron features observed by HYDRA. It is expected that the precipitating suprathermal electrons carrying upward field-aligned currents generated the broadband emissions. In the TIDE observations, we found the variable occurrence of the conics and beams at relatively low energies. This indicates that there were sporadic small parallel electrostatic potential drops below the satellite also during the conic observations. The convection direction measured by EFI varied significantly in the region containing the ion conics and beams. The ionospheric outflows could continuously be energized in the perpendicular direction through wave-particle interaction processes during the transport to higher altitudes and that the conics could be accelerated in the direction parallel to the magnetic field by the potential drops, as discussed by *Miyake et al.* [1993]. More detailed investigations of the bursty electron precipitation events and their cause are required to reveal the generation mechanisms of the UFI conics and low-energy beams and the relations with the electron features. The fast three-dimensional electron measurements by HYDRA may provide more definite conclusions in the near future. Field-aligned currents which can be derived from the Magnetic Field Experiment (MFE) on POLAR would provide specific conclusions regarding the relation of the UFI signatures with the generation mechanism and the free energy source.

Moore et al. [1996] recently studied the ionospheric ion heating in an auroral arc on the basis of the rocket observations at altitudes below 620 km. They concluded that the O^+ ions were preferentially energized to form the TAIs under an arc produced by a potential drop >10 kV, which is consistent with the previous rocket results reported by *Moore et al.* [1986]. Before and during the significant perpendicular heating, the ionospheric ions would also be subject to the small upward acceleration by the ambipolar electric field generated by escaping thermal electrons and photoelectrons. Then, the polar wind component in the low-altitude auroral region, which were slightly accelerated by the ambipolar electric field, could be converted to TAIs by wave-particle interactions, and furthermore, portions of the TAIs or the UFI conics would transform to UFI beams if the parallel potential drop exists above the source region for the polar wind and the TAIs. The ionospheric ions in the auroral oval and the polar cap therefore could be energized by single- or multiple-step processes to form three types of upflowing ion distributions: polar wind, UFI conics, and UFI beams.

The parallel electrostatic potential drop below the satellite could further accelerate the conics to form the beam-type UFIs or elevated UFI conics [*Klumpar et al.*, 1984; *Miyake et al.*, 1996]. In this scenario, the first significant energization of the ionospheric ions is the perpendicular heating at low altitudes, and some of the conical ions may be able to gain the further energy from the parallel electric field at higher altitudes between the topside ionosphere and the satellite. In other words, the source region of the TAIs is not always colocated with the discrete high-energy electron precipitation producing the auroral forms detectable from the POLAR satellite. The visible auroral emissions require additional processes precipitating the auroral electrons into the loss cone in the sharply field-aligned direction.

The clear conic signatures were located at higher latitudes than the auroral arc in the duskside observations of the July 25 event. During the transport of the low-energy upgoing ion conics from the topside ionosphere to the observation altitude (POLAR perigee), the global convection would carry the ions from higher latitudes where they originated to lower latitudes. However, because the ionospheric ions would be continuously accelerated transversely even above the POLAR perigee by wave-particle interaction, the conic signatures observed by POLAR showed a good correlation with the broadband emissions at higher latitudes than the auroral arc. The bursty suprathermal electrons which may lead to the processes causing the UFI conics may be more widely spread than the more field-aligned energetic electron beams producing the bright auroral forms. In the case shown in this paper, the suprathermal electrons were observed in the poleward auroral zone and in the polar cap, that is, at higher latitudes than the discrete (visible) auroral emissions produced by the energetic electron beams.

The TIMAS and HYDRA data on June 12 and July 25 indicated that the discrete auroras were observed on closed field lines since the high-energy diffuse ion and electron features coexisted with the UFI beams and the inverted-V electron events. On the other hand, the conics were always located at the poleward boundary from the discrete features of auroras and UFIs, which may imply that the conics tend to occur in and near the open-closed boundary, like the plasma sheet boundary layer (PSBL). Observations from the Akebono satellite also show that the high-energy conics are more often observed at the poleward boundary of the plasma sheet, which is likely correspondent to the PSBL. The POLAR results with respect to the general auroras and plasma characteristics on the duskside and dawnside are consistent with the Akebono results in the premidnight meridian reported by *Yamamoto et al.* [1993]. Although the beam-like UFIs were at times detected during intervals of conics, the peak energy was lower than that of the UFI beams in the discrete aurora, namely, in the large parallel electrostatic potential drop.

It is generally known that the center of the AKR feature with the lowest frequency has a good correlation with an inverted-V signature at the peak energy. The works by *Benson and Calvert* [1979] and *Benson et al.* [1980] concluded that the AKR signatures correlate with the inverted-V electrons with hole structures and that their intensity depends on the electron density in the source region. In fact, *Huff et al.* [1988] reported that the AKR source regions mapped

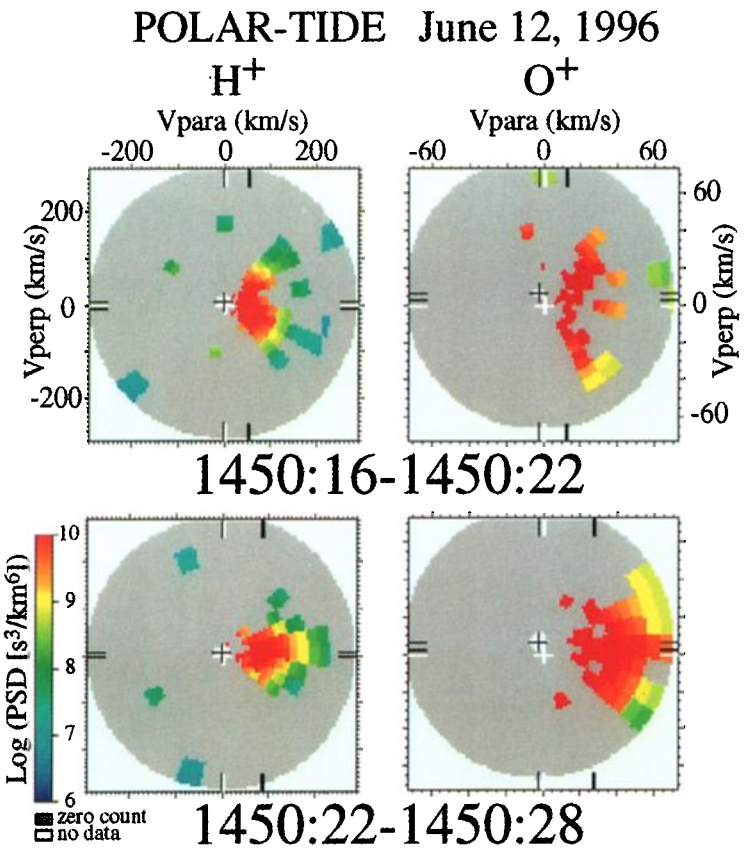

Plate 7. Velocity distribution functions of the low-energy H^+ and O^+ conics and beams observed by TIDE, similar to Plate 2b.

to the portions of bright auroral forms. However, for the POLAR observations presented here, the AKR intensity was not always strongly correlated with the auroral brightness nor the geomagnetic activity. Our results also indicate that the center of the AKR signatures was located at slightly lower latitudes than the inverted-V electron structure and the UFI beam distribution. Recently, *Menietti et al.* [1993] demonstrated the close relation of the AKR with the electron and ion features accelerated by the parallel electrostatic potential drop observed by DE 1. For several cases, the centers of the intense AKR signatures were observed at slightly lower latitudes than the regions with the largest flux and energy of the inverted-V electrons, while the Viking observations presented by *Ungstrup et al.* [1990] showed a colocation of the AKR center with the parallel potential drop. We conclude that our results from POLAR on June 12 are consistent with these DE 1 results and the events by *Benson et al.* [1980].

While *Bahnsen et al.* [1989] reported that the AKR sources were situated on the field lines threading the PSBL, the POLAR data on the duskside and dawnside sectors evidently show that the AKR sources were observed with the UFI beams and auroral forms on the closed field lines significantly equatorward of the PSBL. Also, in the cases shown in this paper, the large parallel electrostatic potential drops causing the intense AKR, high-energy UFI beams, and bright discrete auroras were apparently generated on the closed field lines equatorward of the PSBL on the duskside and dawnside.

The convection directions fluctuated through the regions of the high-energy UFI beams and discrete auroras. In general, the convection reversal occurred in these discrete features. While the convection pattern was also complicated near the UFI conics at higher latitudes, the variations were smaller than those in the regions of the UFI beams and discrete auroras. These results suggest that the convection reversal basically occurs in the plasma sheet equatorward of the PSBL and that the PSBL embeds small distortions in the convection pattern. The convection reversal and small distortions are associated with the high-energy UFI beams in the bright auroral form and the UFI conics without large parallel acceleration, respectively. Since the broadband wave emissions were often observed in the UFI beams and auroras, the initial energization of the ionospheric ions before the formation of the UFI beams would be the heating perpendicular to the local magnetic field. After the perpendicular heating, the UFI conics generated at lower latitudes than the PSBL could be accelerated further at higher altitudes of a few thousands of kilometers by the large parallel electrostatic potential drop.

5. Summary and Conclusions

The POLAR observations represented here can be summarized as follows:

1. The UFI conic signatures correlate well with the auroral hiss emissions and broadband electrostatic emissions and the

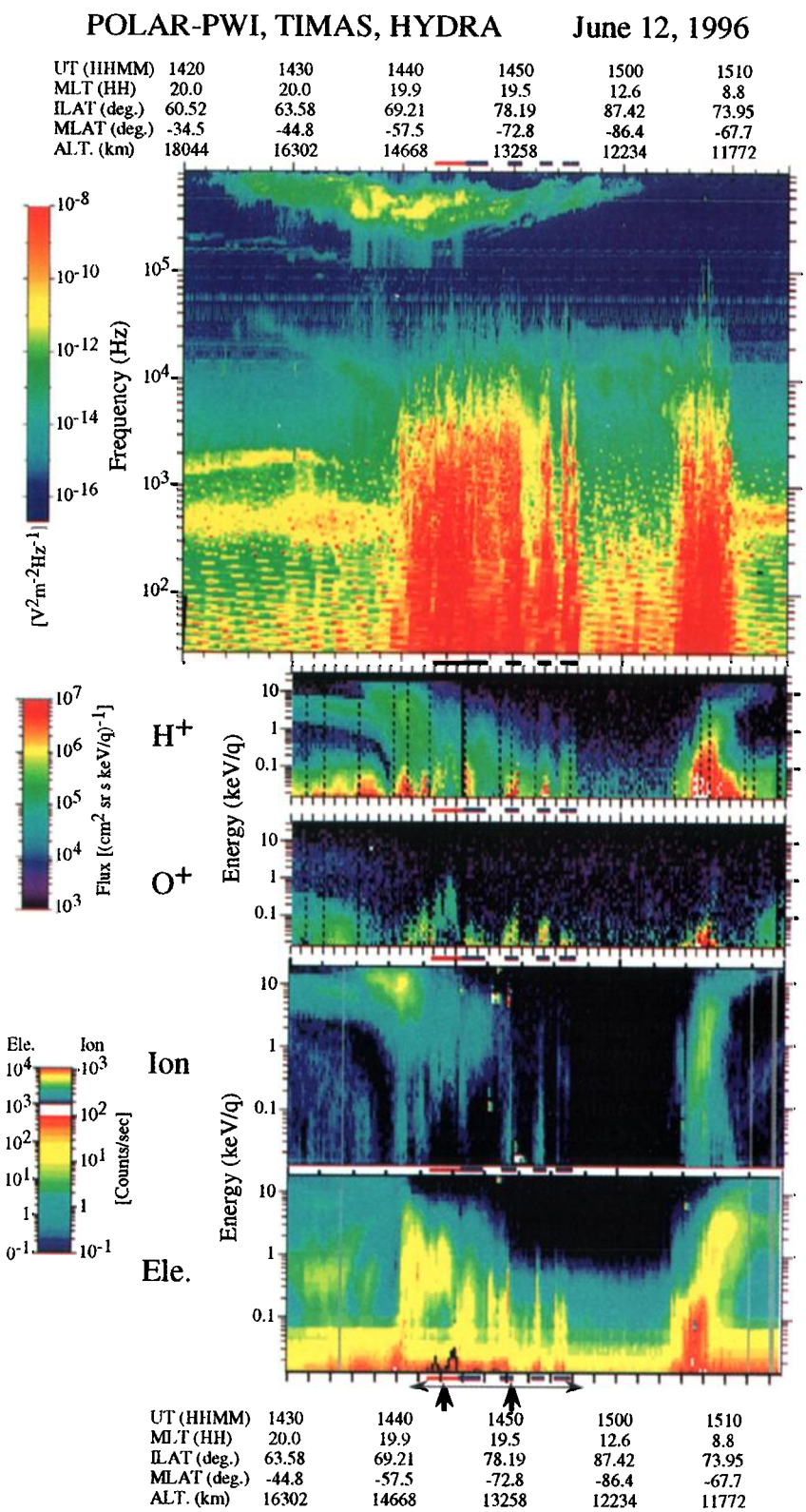

Plate 8. Simultaneous observations by PWI (top panel: *f-t* spectrogram of electric field component), TIMAS (middle two panels: H^+ and O^+ *E-t* spectrograms), HYDRA (bottom two panels: ion and electron *E-t* spectrograms) on June 12, 1996. The data display formats are similar to those of Plate 4. The red and blue underlines near the abscissas are correspondent to the underlines of the same types in Plate 6, indicating the UFI beams (red) and conics (blue). The interval indicated by a horizontal line with arrows at the bottom is the same interval as the TIDE chromograms in Plate 6. The velocity distributions during the intervals indicated by upward arrows are shown in Plates 7 and 9.

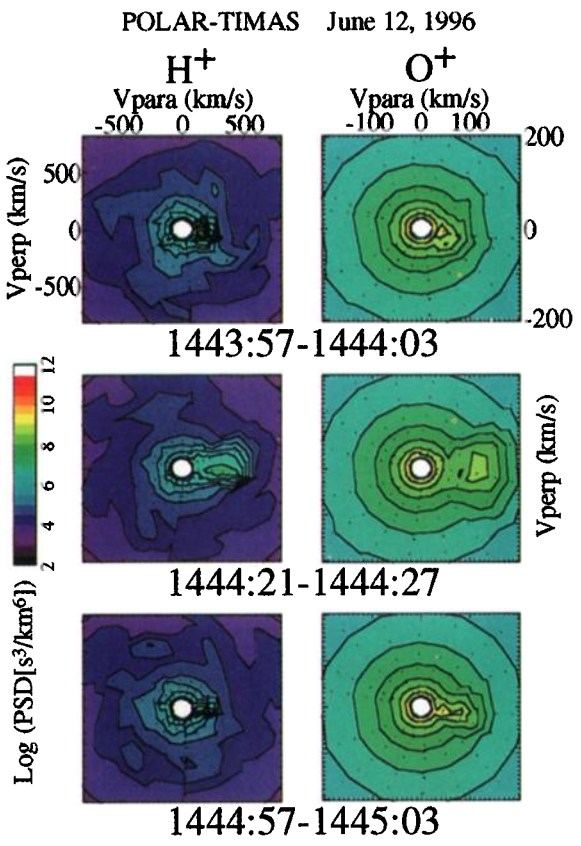

Plate 9. Velocity distribution functions of the H^+ and O^+ beams observed by TIMAS, similar to Plate 2a, but for the UFI beams during the inverted-V event on June 12, 1996.

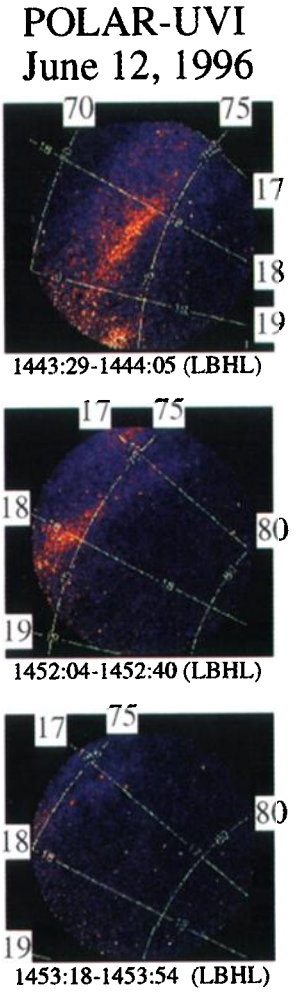

Plate 10. Auroral images observed by UVI, similar to Plate 3, but for the data on June 12, 1996.

low-frequency electric field fluctuations observed by PWI and EFI, respectively. No significant auroral emissions were detected in the region with the conics.

2. The UFI beams which were probably produced by parallel electric fields below the satellite were associated with bright discrete auroral signatures and intense AKR signatures observed over wide frequency ranges.

3. The conics were often observed at higher latitudes than the beams, the auroral forms, and the center of the AKR signatures. The upgoing ionospheric ion energy and angular distribution gradually changed from the conic distributions to the polar wind components at higher latitudes in the polar cap.

4. When the parallel electrostatic potential drop produced the auroral form, the ionospheric ions could be accelerated upward by the parallel electric field during or after the energization perpendicular to the local magnetic field at low altitudes.

As discussed in several previous papers, it is highly plausible that the low-frequency waves and/or fluctuations observed by PWI and EFI energize the ionospheric ions in the perpendicular direction to the local magnetic field. Nevertheless, no significant auroral forms are correlated with the conic signatures and the low-frequency wave activities. It is expected that auroral forms detectable by UVI are not necessarily related to the conics nor the processes producing the TAI. In the bright discrete auroral region, the parallel electrostatic potential drop accelerated the ionospheric low-energy UFI conics to the higher-energy field-aligned beams. The discrete auroral form, UFI beams, and high-frequency electromagnetic AKR were produced by the electrostatic potential drop, which could accelerate the conics further in the parallel direction.

Acknowledgments.

We thank V. Coffey for her efforts on TIDE calibration. We are grateful to P. Sloan and R. West for development of the TIDE software. G. K. Parks, the principal investigator of UVI, kindly allowed us to include UVI images in this paper. R. P. Lepping and K. W. Ogilvie provided us with their Wind data to monitor the IMF and solar wind conditions, respectively. The Kakioka Magnetic Observatory provided the ground magnetogram data. M. H. is grateful to D. L. Gallagher for valuable discussions on the AKR signatures. We acknowledge that the works regarding the instrument developments and data processing were supported under NASA grants NAG8-114, NAG8-693, NASA contract NAS8-38189, and SwRI Internal Research Project 15-9455 for TIDE, NASA contract NAS5-30302 at Lockheed for TIMAS, NASA contract NAS8-38145 and NAS8-38146 at NASA-MSFC and the University of Alabama for UVI, NASA contract NAS5-30371 at the University of Iowa for PWI, NASA contract NAS5-30367 and NASA grant number NAG5-3182 at the University of California and at Mission Research Corporation.

for EFI. This work was also supported by the NASA GGS Project, Office of Space Science, under UDN 370-17-43, and by the NASA Marshall Space Flight Center.

The Editor thanks A. W. Yau, J. A Slavin, and another referee for their assistance in evaluating this paper.

References

Akasofu, S.-I., The dynamical morphology of the aurora polaris, *J. Geophys. Res., 68*, 1667-1673, 1963.

Akasofu, S.-I., The development of the auroral substorm, *Planet. Space Sci., 12*, 273-282, 1964.

Abe, T., B. A. Whalen, A. W. Yau, R. E. Horita, S. Watanabe, and E. Sagawa, EXOS-D (Akebono) SMS observations of the polar wind, *J. Geophys. Res., 98*, 11,191-11,203, 1993a.

Abe, T., B. A. Whalen, A. W. Yau, S. Watanabe, E. Sagawa, and K. I. Oyama, Altitude profile of the polar wind velocity and its relationship to ionospheric conditions, *Geophys. Res. Lett., 20*, 2825-2828, 1993b.

André, M., H. Koskinen, G. Gustafsson, and R. Lundin, Ion waves and upgoing ion beams observed by the Viking satellite, *Geophys. Res. Lett., 14*, 463-466, 1987.

André, M., H. Koskinen, L. Matson, and R. Erlandson, Local transverse ion energization in and near the polar cusp, *Geophys. Res. Lett., 15*, 107-110, 1988.

André, M., G. B. Crew, W. K. Peterson, A. M. Persoon, C. J. Pollock, and M. J. Engebretson, Ion heating by broadband low-frequency waves in the cusp/cleft, *J. Geophys. Res., 95*, 20,809-20,823, 1990.

André, M., P. Norqvist, A. Vaivads, L. Eliasson, O. Norberg, A. Eriksson, and B. Holback, Transverse ion energization and wave emissions observed by the Freja satellite, *Geophys. Res. Lett., 21*, 1915-1918, 1994.

Balsiger, H., P. Eberhardt, J. Geiss, and D. T. Young, Magnetic storm injection of 0.9- to 16 keV/*e* solar and terrestrial ions into the high-altitude magnetosphere, *J. Geophys. Res., 85*, 1645-1662, 1980.

Banks, P. M., and T. E. Holzer, The polar wind, *J. Geophys. Res., 73*, 6846-6854, 1968.

Bahnsen, A., B. M. Pedersen, M. Jespersen, E. Ungstrup, L. Eliasson, J. S. Murphree, R. D. Elphinstone, L. Blomberg, G. Holmgren, and L. J. Zanetti, Viking observations at the source region of auroral kilometric radiation, *J. Geophys. Res., 94*, 6643-6654, 1989.

Benson, R. F., and W. Calvert, ISIS 1 observations at the source of auroral kilometric radiation, *Geophys. Res. Lett., 6*, 479-482, 1979.

Benson, R. F., W. Calvert, and D. M. Klumpar, Simultaneous wave and particle observations in the auroral kilometric radition source region, *Geophys. Res. Lett., 7*, 959-962, 1980.

Bosqued, J. M., C. Maurel, J. A. Sauvaud, R. A. Kavrazhkin, and Y. I. Galperin, Observations of auroral electron inverted-V structures by the Aureol-3 satellite, *Planet. Space Sci., 34*, 255-269, 1986.

Chappell, C. R., T. E. Moore, and J. H. Waite Jr., The ionosphere as a fully adequate source of plasma for the Earth's magnetosphere, *J. Geophys. Res., 92*, 5896-5910, 1987.

Chandler, M. O., J. H. Waite Jr., and T. E. Moore, Observations of polar ion outflows, *J. Geophys. Res., 96*, 1421-1428, 1991.

Chang, T., G. B. Crew, N. Hershkowitz, J. R. Jasperse, J. M. Retterer, and J. D. Winningham, Transverse acceleration of oxygen ions by electromagnetic ion cyclotron resonance with broad band left-hand polarized waves, *Geophys. Res. Lett., 13*, 636-639, 1986.

Chen, M. W., W. K. Peterson, M. Ashour-Abdalla, T. E. Moore, and A. M. Persoon, Plasma characteristics of upflowing ion beams in the polar cap region, *J. Geophys. Res., 95*, 3907-3924, 1990.

Collin, H. L., R. D. Sharp, E. G. Shelley, and R. G. Johnson, Some general characteristics of upflowing ion beams over the auroral zone and their relationship to auroral electrons, *J. Geophys. Res., 86*, 6820-6826, 1981.

Crew, G. B., T. Chang, J. M. Retterer, W. K. Peterson, D. A. Gurnett, and R. L. Huff, Ion cyclotron resonance heated conics: Theory and observations, *J. Geophys. Res., 95*, 3959-3985, 1990.

Craven, J. D., and L. A. Frank, The temporal evolution of a small auroral substorm as viewed from high altitude with Dynamics Explorer 1, *Geophys. Res. Lett., 12*, 465-468, 1985.

Craven, J. D., and L. A. Frank, Latitudinal motions of the aurora during substorms, *J. Geophys. Res., 92*, 4565-4573, 1987.

Elphinstone, R. D., and D. J. Hearn, Mapping of the auroral distribution during quiet times and substorm recovery, *Proceeding of the First ICS-1, Eur. Space Agency Spec. Publ., 335*, 13-18, 1992.

Elphinstone, R. D., and D. J. Hearn, The auroral distribution and its relation to magnetospheric processes, *Adv. Space Res., 13* (4), 17-27, 1993.

Elphinstone, R. D., et al., Observations in the vicinity of substorm onset: Implications for the substrom process, *J. Geophys. Res., 100*, 7937-7969, 1995a.

Elphinstone, R. D., et al., The double oval UV auroral distribution, 1, Implications for the mapping of auroral arcs, *J. Geophys. Res., 100*, 12,075-12,092, 1995b.

Elphinstone, R. D., et al., The double oval UV auroral distribution, 2, The most poleward arc system and the dynamics of the magnetotail, *J. Geophys. Res., 100*, 12,093-12,102, 1995c.

Erlandson, R. E., L. J. Zanetti, M. H. Acuña, A. I. Eriksson, L. Eliasson, M. H. Boehm, and L. G. Blomberg, Freja observations of electromagnetic ion cyclotron ELF waves and transverse oxygen ion acceleration on auroral field lines, *Geophys. Res. Lett., 21*, 1855-1858, 1994.

Frank, L. A., and K. L. Ackerson, Observations of charge particle precipitation into the auroral zone, *J. Geophys. Res., 76*, 3612-3643, 1971.

Ghielmetti, A. G., R. D. Sharp, E. G. Shelley, and R. G. Johnson, Downward flowing ions and evidence for injection of ionospheric ions into the plasma sheet, *J. Geophys. Res., 84*, 5781-5791, 1979.

Green, J. L., D. A. Gurnett, and R. A. Hoffman, A correlation between auroral kilometric radiation and inverted V electron precipitation, *J. Geophys. Res., 84*, 5216-5222, 1979.

Gurnett, D. A., Auroral plasma waves, in *Auroral Physics*, p. 241, Cambrige Univ. Press, New York, 1991.

Gurnett, D. A., et al., The POLAR plasma wave instrument, *Space Sci. Rev., 71*, 597-622, 1995.

Harvey, P., et al., The electric field instrument on the POLAR satellite, *Space Sci. Rev., 71*, 583-596, 1995.

Henderson, M. G., J. S. Murphree, and J. M. Weygand, Observations of auroral substorms occurring together with preexisting "quiet time" auroral patterns, *J. Geophys. Res., 101*, 24,621-24,640, 1996.

Heppner, J. P., and N. C. Maynard, Empirical high-latitude electric field models, *J. Geophys. Res., 92*, 4467-4489, 1987.

Horwitz, J. L., The ionosphere as a source of magnetospheric ions, *Rev. Geophys., 20*, 929-952, 1982.

Horwitz, J. L., Velocity filter mechanism for ion bowl distributions (bimodal conics), *J. Geophys. Res., 91*, 4513-4523, 1986.

Horwitz, J. L., C. J. Pollock, T. E. Moore, W. K. Peterson, J. L. Burch, J. D. Winningham, J. D. Craven, L. A. Frank, and A. Persoon, The polar cap environment of outflowing O^+, *J. Geophys. Res., 97*, 8361-8379, 1992.

Huff, R. L., W. Calvert, J. D. Craven, L. A. Frank, and D. A. Gurnett, Mapping of auroral kilomentric radiation sources to the aurora, *J. Geophys. Res., 93*, 11,445-11,454, 1988.

Hultqvist, B., On the acceleration of positive ions by high-latitude, large-amplitude electric field fluctuations, *J. Geophys. Res., 101*, 27,111-27,121, 1996.

Hultqvist, B., R. Lundin, K. Stasiewicz, L. Block, P.-A. Lindqvist, G. Gustafsson, H. Koskinen, A. Bahnsen, T. A. Potemra, and L. J. Zanetti, Simultaneous observation of upward moving field-

aligned energetic electrons and ions on auroral zone field lines, *J. Geophys. Res., 93*, 9765-9776, 1988.

Johnson, R. G., Energetic ion composition in the Earth's magnetosphere, *Rev. Geophys., 17*, 696-705, 1979.

Kintner, P. M., and D. J. Gorney, A search for the plasma processes associated with perpendicular ion heating, *J. Geophys. Res., 89*, 937-944, 1984.

Kintner, P. M., W. Scales, J. Vago, R. Arnoldy G. Garbe, and T. Moore, Simultaneous observations of electrostatic oxygen cyclotron waves and ion conics, *Geophys. Res. Lett., 16*, 739-742, 1989.

Kintner, P. M., J. Bonnell, R. Arnoldy, K. Lynch, C. Pollock, and T. Moore, SCIFER - Transverse ion acceleration and plasma waves, *Geophys. Res. Lett., 23*, 1873-1876, 1996.

Klumpar, D. M., W. K. Peterson, and E. G. Shelley, Direct evidence for two-stage (bimodal) acceleration of ionospheric ions, *J. Geophys. Res., 89*, 10,779-10,787, 1984.

Kondo, T., B. A. Whalen, A. W. Yau, and W. K. Peterson, Statistical analysis of upflowing ion beam and conic distributions at DE 1 altitudes, *J. Geophys. Res., 95*, 12,091-12,102, 1990.

Lepping, R. P., et al., The WIND magnetic field investigation, *Space Sci. Rev., 71*, 207-229, 1995.

Liu, C., J. D. Perez, T. E. Moore, and C. R. Chappell, Boundary structure of low-energy ions associated with the nightside convection reversal, *J. Geophys. Res., 99*, 11,401-11,409, 1994a.

Liu, C., J. D. Perez, T. E. Moore, C. R. Chappell, and J. A. Slavin, Fine structure of low-energy H^+ in the nightside auroral region, *J. Geophys. Res., 99*, 4131-4141, 1994b.

Lennartsson, W., R. D. Sharp, and R. D. Zwickl, Substorm effects on the plasma sheet ion composition on March 22, 1979 (CDAW 6), *J. Geophys. Res., 90*, 1243-1252, 1985.

Lockwood, M., J. H. Waite Jr., J. F. E. Johnson, T. E. Moore, and C. R. Chappell, A new source of suprathermal O^+ ions near the dayside polar cap boundary, *J. Geophys. Res., 90*, 4099-4116, 1985.

Lu, G., P. H. Reiff, T. E. Moore, and R. A. Heelis, Upflowing ionospheric ions in the auroral region, *J. Geophys. Res., 97*, 16,855-16,863, 1992.

Lundin, R., B. Hultqvist, E. Dubinin, A. Zackarov, and N. Pissarenko, Observations of outflowing ion beams on auroral field lines at altitudes of many Earth radii, *Planet. Space Sci., 30*, 715-726, 1982.

Lundin, R., and B. Hultqvist, Ionospheric plasma escape by high-altitude electric field: Magnetic moment "pumping," *J. Geophys. Res., 94*, 6665-6680, 1989.

Menietti, J. D., J. L. Burch, R. M. Winglee, and D. A. Gurnett, DE 1 particle and wave observations in auroral kilometric radiation (AKR) source regions, *J. Geophys. Res., 98*, 5865-5879, 1993.

Miyake, W., T. Mukai, and N. Kaya, On the evolution of ion conics along the field line from EXOS D observations, *J. Geophys. Res., 98*, 11,127-11,134, 1993.

Miyake, W., T. Mukai, and N. Kaya, On the origins of the upward shift of elevated (bimodal) ion conics in velocity space, *J. Geophys. Res., 101*, 26,961-26,969, 1996.

Moore, T. E., C. R. Chappell, M. Lockwood, and J. H. Waite Jr., Superthermal ion signatures of auroral acceleration processes, *J. Geophys. Res., 90*, 1611-1618, 1985.

Moore, T. E., C. J. Pollock, R. L. Arnoldy, and P. M. Kintner, Preferential O^+ heating in the topside ionosphere, *Geophys. Res. Lett., 13*, 901-904, 1986.

Moore, T. E., et al., The thermal ion dynamics experiment and plasma source instrument, *Space Sci. Rev., 71*, 409-458, 1995.

Moore, T. E., M. O. Chandler, C. J. Pollock, D. L. Reasoner, R. L. Arnoldy, B. Austin, P. M. Kintner, and J. Bonnell, Plasma heating and flow in an auroral arc, *J. Geophys. Res., 101*, 5279-5297, 1996.

Nagai, T., J. H. Waite Jr., J. L. Green, C. R. Chappell, R. C. Olsen, and R. H. Comfort. First measurements of supersonic polar wind in the polar magnetosphere, *Geophys. Res. Lett., 11*, 669-672, 1984.

Norqvist, P., M. André, L. Eliasson, A. I. Eriksson, L. Blomberg, H. Lühr, and J. H. Clemmons, Ion cyclotron heating in the dayside magnetosphere, *J. Geophys. Res., 101*, 13,179-13,193, 1996.

Ogilvie, K. W., et al., SWE, A comprehensive plasma instrument for the WIND spacecraft, *Space Sci. Rev., 71*, 55-77, 1995.

Peterson, W. K., R. D. Sharp, E. G. Shelley, and R. G. Johnson, Energetic ion composition of the plasma sheet, *J. Geophys. Res., 86*, 761-767, 1981.

Peterson, W. K., E. G. Shelley, S. A. Boardsen, D. A. Gurnett, B. G. Ledley, M. Sugiura, T. E. Moore, and J. H. Waite, Transverse ion energization and low-frequency plasma waves in the mid-altitude auroral zone: A case study, *J. Geophys. Res., 93*, 11,405-11,428, 1988.

Pollock, C. J., M. O. Chandler, T. E. Moore, J. H. Waite Jr., C. R. Chappell, and D. A. Gurnett, A survey of upwelling ion event characteristics, *J. Geophys. Res., 95*, 18,969-18,980, 1990.

Reiff, P. H., H. L. Collin, J. D. Craven, J. L. Burch, J. D. Winningham, E. G. Shelley, L. A. Frank, and M. A. Friedman, Determination of auroral electostatic potentials using high- and low-altitude particle distributions, *J. Geophys. Res., 93*, 7441-7465, 1988.

Scudder, J., et al., HYDRA - A 3-dimensional electron and ion hot plasma instrument for the Polar spacecraft of the GGS, *Space Sci. Rev., 71*, 459-495, 1995.

Sharp, R. D., D. L. Carr, W. K. Peterson, and E. G. Shelley, Ion streams in the magnetotail, *J. Geophys. Res., 86*, 4639-4648, 1981.

Sharp, R. D., W. Lennartsson, W. K. Peterson, and E. G. Shelley, The origin of the plasma in the distant plasma sheet, *J. Geophys. Res., 87*, 10,420-10,424, 1982.

Shelley, E. G., W. K. Peterson, A. G. Ghielmetti, and J. Geiss, The polar ionosphere as a source of energetic magnetospheric plasma, *Geophys. Res. Lett., 9*, 941-944, 1982.

Shelley, E. G., et al., The toroidal imaging mass-angle spectrograph (TIMAS) for the POLAR mission, *Space Sci. Rev., 71*, 497-530, 1995.

Temerin, M., F. S. Mozer, and D. Gurnett, Large amplitude ion cyclotron waves detected by Polar, *Eos Trans. AGU, 77*, 620, 1996.

Torr, M. R., et al., A far ultraviolet image for the international solar-terrestrial physics mission, *Space Sci. Rev., 71*, 329-383, 1995.

Ungstrup, E., A. Bahnsen, H. K. Wong, M. André, and L. Matson, Energy source and generation mechanism for auroral kilometric radiation, *J. Geophys. Res., 95*, 5973-5981, 1990.

Waite, J. H., Jr., T. Nagai, J. F. E. Johnson, C. R. Chappell, J. L. Burch, T. L. Killeen, P. B. Hays, G. R. Carignan, W. K. Peterson, and E. G. Shelley, Escape of suprathermal O^+ ions in the polar cap, *J. Geophys. Res., 90*, 1619-1630, 1985.

Yamamoto, T., E. Kaneda, H. Hayakawa, T. Mukai, A. Matsuoka, S. Machida, H. Fukunishi, N. Kaya, K. Tsuruda, and A. Nishida, Meridional structures of electric potentials relevant to premidnight dicrete auroras: A case study from Akebono measurements, *J. Geophys. Res., 98*, 11,135-11,151, 1993.

Yau, A. W., B. A. Whalen, W. K. Peterson, and E. G. Shelley, Distribution of upflowing ionospheric ions in the high-altitude polar cap and auroral ionosphere, *J. Geophys. Res., 89*, 5507-5522, 1984.

Yau, A. W., E. G. Shelley, W. K. Peterson, and L. Lenchyshyn, Energetic auroral and polar ion outflow at DE 1 altitudes: Magnitude, composition, magnetic activity dependence, and long-term variation, *J. Geophys. Res., 90*, 8417-8432, 1985.

Young, D. T., H. Balsiger, and J. Geiss, Correlations of magnetospheric ion composition with geomagnetic and solar activity, *J. Geophys. Res., 87*, 9077-9096, 1982.

M. J. Brittnacher, Geophysics Program, University of Washington, Seattle, WA 98195. (e-mail: britt@geophys.washington.edu)

M. O. Chandler, P. D. Craven, B. L. Giles, and J. F. Spann, Space Sciences Laboratory Code ES-83, NASA Mar-

shall Space Flight Center, Huntsville, AL 35812. (e-mail: michael.chandler@msfc.nasa.gov; paul.craven@msfc.nasa.gov; barbara.giles@msfc.nasa.gov; jim.spann@msfc.nasa.gov)

G. A. Germany, and J. L. Horwitz, Center of Space Plasma, Aeronomy, and Astrophysics Research, University of Alabama in Huntsville, AL 35899. (e-mail: germanyg@cspar.uah.edu; horwitzj@cspar.uah.edu)

D. A. Gurnett, A. M. Persoon, J. S. Pickett, and J. D. Scudder, Department of Physics and Astronomy, University of Iowa, Iowa City, IA 52242. (e-mail: gurnett@iowave.physics.uiowa.edu; persoon@iowave.physics.uiowa.edu; pickett@iowave.physics.uiowa.edu; jds@space-theory.physics.uiowa.edu)

M. Hirahara, Department of Physics, College of Science, Rikkyo University, 3-34-1 Nishi-Ikebukuro, Toshima-ku, Tokyo 171, Japan. (e-mail: hirahara@se.rikkyo.ac.jp)

N. C. Maynard, Mission Research Corporation, One Tara Blvd., Ste 302, Nashua, NH 03062. (e-mail: nmaynard@mrcnh.com)

T. E. Moore, Interplanetary Physics Branch, NASA Goddard Space Flight Center, Greenbelt, MD 20771. (e-mail: T.E.moore@gsfc.nasa.gov)

F. S. Mozer, Space Sciences Laboratory, University of California, Berkeley, CA 94720. (e-mail: fmozer@sunspot.ssl.berkeley.edu)

C. J. Pollock, Instrumentation and Space Research Division, Southwest Research Institute, PO Drawer 28510, San Antonio, TX 78228. (e-mail: cpollock@swri.edu)

T. Nagai, Planetary and Earth Sciences, Tokyo Institute of Technology, 2-12-1 Ookayama, Meguro-ku, Tokyo 152, Japan. (e-mail: nagai@geo.titech.ac.jp)

W. K. Peterson, and E. G. Shelley, Lockheed Martin Space Physics Laboratory, Dept. 91-20, Building 252, 3251 Hanover Street, Palo Alto, CA 94304. (e-mail: pete@space.lockheed.com; shelley@space.lockheed.com)

(Received March 20, 1997; revised September 17, 1997; accepted September 18, 1997.)